University of Denver
Digital Commons @ DU

Electronic Theses and Dissertations | Graduate Studies

1-1-2012

Aladdin's Magic Lamp: Developing Methods for Calibration and Geolocation Accuracy Assessment of the DMSP OLS

Benjamin Taylor Tuttle
University of Denver

Follow this and additional works at: https://digitalcommons.du.edu/etd

 Part of the Geographic Information Sciences Commons, and the Remote Sensing Commons

Recommended Citation

Tuttle, Benjamin Taylor, "Aladdin's Magic Lamp: Developing Methods for Calibration and Geolocation Accuracy Assessment of the DMSP OLS" (2012). *Electronic Theses and Dissertations*. 941.
https://digitalcommons.du.edu/etd/941

This Dissertation is brought to you for free and open access by the Graduate Studies at Digital Commons @ DU. It has been accepted for inclusion in Electronic Theses and Dissertations by an authorized administrator of Digital Commons @ DU. For more information, please contact jennifer.cox@du.edu,dig-commons@du.edu.

ALADDIN'S MAGIC LAMP: DEVELOPING METHODS FOR CALIBRATION AND GEOLOCATION ACCURACY ASSESSMENT OF THE DMSP OLS

_____

A Dissertation

Presented to

the Faculty of Natural Sciences and Mathematics

University of Denver

_____

In Partial Fulfillment

of the Requirements for the Degree

Doctor of Philosophy

_____

by

Benjamin Taylor Tuttle

June 2012

Advisor: Sharolyn Anderson

Author: Benjamin Taylor Tuttle
Title: ALADDIN'S MAGIC LAMP: DEVELOPING METHODS FOR CALIBRATION AND GEOLOCATION ACCURACY ASSESSMENT OF THE DMSP OLS
Advisor: Sharolyn Anderson
Degree Date: June 2012

Abstract

Nighttime satellite imagery from the Defense Meteorological Satellite Program (DMSP) Operational Linescan System (OLS) has a unique capability to observe nocturnal light emissions from sources including cities, wild fires, and gas flares. Data from the DMSP OLS is used in a wide range of studies including mapping urban areas, estimating informal economies, and estimating urban populations. Given the extensive and increasing list of applications a repeatable method for assessing geolocation accuracy, performing inter-calibration, and defining the minimum detectable brightness would be beneficial. An array of portable lights was designed and taken to multiple field sites known to have no other light sources. The lights were operated during nighttime overpasses by the DMSP OLS and observed in the imagery. A first estimate of the minimum detectable brightness is presented based on the field experiments conducted. An assessment of the geolocation accuracy was performed by measuring the distance between the GPS measured location of the lights and the observed location in the imagery. A systematic shift was observed and the mean distance was measured at 2.9km. A method for in situ radiance calibration of the DMSP OLS using a ground based light source as an active target is presented. The wattage of light used by the active target strongly correlates with the signal measured by the DMSP OLS. This approach can be used to enhance our ability to make inter-temporal and inter-satellite comparisons of DMSP OLS imagery. Exploring the possibility of establishing a permanent active target

for the calibration of nocturnal imaging systems is recommended. The methods used to assess the minimum detectable brightness, assess the geolocation accuracy, and build inter-calibration models lay the ground work for assessing the energy expended on light emitted into the sky at night. An estimate of the total energy consumed to light the night sky globally is presented.

Acknowledgements

This research was funded in part by and NASA Earth and Space Science Fellowship and an ASPRS Rocky Mountain Region Scholarship. I wish to thank all the individuals at the Colorado Division of Wildlife and the National Forest Service who helped to organize access to the field sites and the Air Force Weather Agency for their support. I have had a great deal of amazing teachers over the years helping to prepare me for this challenge and would not have made it here without them. I also wish to thank all my friends for their support and encouragement. Additionally, thank you to all the individuals who assisted in the various field expeditions.

I would like to thank Sharolyn Anderson for her constant encouragement and guidance along the way and for helping me keep this project on track, I could not have asked for a better advisor. I also wish to thank my committee members Paul Sutton, Chris Elvidge, and Becky Powell for their numerous insights, comments, and support. I must also thank Kim Baugh from the National Geophysical Data Center for her support throughout this process.

I could not have completed this endeavor without the support of my parents and siblings. I consider myself very lucky to have such an amazing, supportive, and loving family. I would also like to recognize Bob Feden, a close friend of the family, and personal mentor to me.

Lastly, special thanks go to Kristina Yamamoto who has been a constant source of support and inspiration on this journey. She has graciously endured numerous outings to the cold dark corners that I call field sites. She made this experience more manageable in the hard times and more fun in the good times.

Table of Contents

Chapter One: Introduction

Background

The U.S. Air Force Defense Meteorological Satellite Program (DMSP) Operational Linescan System (OLS) has a unique capability for low light imaging of the earth at night. The OLS acquires data in two spectral bands: visible and thermal. DMSP satellites are in a sun-synchronous, low altitude polar orbit. At night the visible band signal is intensified using a photomultiplier tube (PMT) to enable detection of moonlit clouds. Though not designed for this purpose, the OLS produces the only nightly global imagery of lighting present at the earth's surface. The National Geophysical Data Center (NGDC) operates the long term archive for OLS data and has worked for 17 years to develop the algorithms and processing capability for constructing global cloud-free composites of nighttime lights (Elvidge et al., 1997a; Elvidge et al., 2001b). The OLS detects four primary types of lighting: human settlements (cities, towns, and villages), fires, gas flares, and heavily lit fishing boats. OLS nighttime lights data have been used for estimations of population and energy consumption (Elvidge et al., 1997c), estimation of forest area impacted by wild fires (Elvidge et al., 2001a), estimating impervious surface area (Elvidge et al., 2004a; Elvidge et al., 2007d), modeling population density (Sutton, 1997; Sutton et al., 2003), studies of net primary productivity and carbon modeling (Milesi et al., 2003; Milesi et al., 2005). NGDC offers a time series of global nighttime lights from 1992 to 2010 using data from the four DMSP satellites that

collected nighttime data during this time period. These are available at: http://www.ngdc.noaa.gov/dmsp/downloadV4composites.html.

The products generated form DMSP OLS data are used in a wide array of research areas. One research topic that has made extensive use of nighttime lights is the mapping of urban extents. There is a general consensus that over the past 30 years the world's population has had the highest absolute increase of any period in human history, although exact numbers are elusive. Currently, around 50% of the world's population lives in urban areas (United-Nations-Population-Fund, 2008). Projections suggest that by 2030 this number could rise to 61% and most of this growth will occur in less developed countries (Fragkias & Seto, 2007). As the world's population increases and existing urban areas expand, along with the emergence of new urban areas, the current landscape will be changed dramatically.

Remote Sensing of Urban Areas

Remotely sensed data from multiple sensors has been used in a number of ways to measure the spatial extent of urbanization. There is a need for more consistent data on urban areas and there have been many studies using remotely sensed data to this end. However, defining urban areas with remotely sensed data is a difficult task. Two reasons for this are that urban areas are usually a mix of materials, including natural materials such as grass, trees and soils, as well as impervious surfaces such as concrete and asphalt, which can make urban land cover difficult to identify (Powell et al., 2007). This problem is lessened by high resolution (<5m) satellite imagery, however it does not solve all the problems and due to the cost and effort involved in identifying urban areas with such

imagery it is prohibitive for anything other than small areas (Elvidge et al., 2004c). There are also some difficulties with determining the definition of urban which further confuse the issue. Producing more consistent data on urban areas as well as the use of remote sensing in mapping urban areas is a topic of great importance given current trends.

Urban areas may be defined in many ways and defining them can be difficult (Weeks, 1999). In the context of this research the following definition is suitable "Urban places may be broadly defined as the settlements where most people live and work" (Elvidge et al., 2004c). However, the exact number of people and landscape altering changes that define urban areas change from region to region and can be difficult to define. Elvidge et al (2004c) define urbanization as the environment altering activities that create and maintain urban areas including construction, habitation, transportation, energy and water use, communication, industrialization, commercial and manufacturing services, as well as civic activities linked to education and governance. In addition to the projected increase in urban extent there are also currently strong trends of development in suburban and exurban areas (Elvidge et al., 2004c; Sutton et al., 2006). The suburban and exurban developments at the urban fringe are often the most obvious signs of growth; however, urban areas tend to constantly evolve due to redevelopment and the replacement of aging infrastructure (Elvidge et al., 2004c).

The concerns about urbanization are compounded by the nature of the process. Most ecological disturbances, such as wildfire, are followed by a period of succession (e.g. Lyon & Stickney, 1976; Turner et al., 1997). In this case the ecosystem continues on its natural path. However, the processes involved in urbanization involved various constructed surfaces, many of them impervious, and designed to last for long periods of

time. Additionally, the products of urbanization, such as roads, are often kept up through maintenance and redevelopment in the urban areas. This means urban areas restrict natural biological succession and ecological recovery (Elvidge et al., 2004c; Elvidge et al., 2007d). This demonstrates another of the reasons it is important to have a solid understanding of urbanization and the areas it affects.

The projected increases in urban populations and the severe impacts on the ecosystems in which urbanization occurs are not the only reasons it is important to understand the location, extent, and trajectory of urbanization. Policymakers in the developing world are faced with increasing pressure to provide assessments of their land use strategies as high population growth is projected for at least the next 25 years (Fragkias & Seto, 2007). To date there has been significant interest in studying megacities (cities with a population of 10 million or more), but much of the projected growth will take place in developing countries (Fragkias & Seto, 2007). There is a need for more detailed studies in the developing world and of cities at scales below the megacity.

Fragkias and Seto (2007) discuss several of the challenges to be overcome in producing better urban land use change models in the developing world. Often studies take place at scales that are not in line with the size of the administrative areas for which policymakers are responsible. Sometimes a dearth of applicable or valid data exists in the developing world for use in modeling urban land use change. Socioeconomic data can range from non-existent to unreliable and the uncertainty can be difficult to characterize compared with remotely sensed data. There is a void to be filled and remote sensing will likely provide a significant contribution.

The definitions of urban and urbanization used above suggest that both numbers of people and constructed surfaces play a role in locating urban areas. To date a number of data sets have been produced, some using just remotely sensed data and others using combinations of remotely sensed data and population data. Nighttime lights data (Elvidge et al., 2001b) have been used by many researchers to map urban area and have also been used as an input to several urban area products derived from multiple sources. Several of these studies will be briefly described.

A model for estimating ambient population globally was released as a product called Landscan (Bhaduri et al., 2002). Population density is an important factor to consider in examining urban areas. This dataset uses not only census counts, which only give an indicator of where people live, but uses a number of inputs to model where people live and work resulting in a representation of population that better reflects the distribution of people around the world. Landscan uses the best available census counts in conjunction with land cover, roads, slope, and nighttime lights (nighttime lights were always used initially, but have not been used in all recent versions such as Landscan 2004). This can help avoid a circular approach when combining Landscan with other urban area products many of which use nighttime lights. The Landscan data set is released at a grid resolution of 30 arc-seconds and has been used in a wide range of applications including counter-terrorism, homeland security, emergency planning and management, consequence analysis, epidemiology, exposure analysis, and urban sprawl detection.

The GRUMP database (Balk et al., 2005; Balk & Yetman, 2004; Balk et al., 2010) developed by Center for International Earth Science Information Network

(CIESIN), Columbia University provides a population dataset, a human settlements (point based) dataset, and an urban areas dataset (CIESIN et al., 2004). The urban areas dataset is derived by starting from the human settlements layer and using nighttime lights and Digital Chart of the World Populated Places data to define the extent of urban areas. This dataset is also distributed at a grid resolution of 30 arc-seconds.

Another urban area product created at Boston University and derived from multiple sources is described by Schneider et al (2003). Their aim was to create a map of urban areas from multiple coarse resolution remotely sensed datasets, which they refer to as a fusion map. The product was created from nighttime lights data, gridded population density data, National Land Cover Data (from the United States Geological Survey), Moderate Resolution Imaging Spectroradiometer (MODIS) Imagery, and training data selected by the Boston University Landcover team. These data were combined into a 1km resolution grid for distribution.

The History Database of the Global Environment (HYDE) is a historical landcover database and was initially developed to test and validate the Integrated Model to Assess the Global Enviroment (Goldewijk, 2001; Goldewijk & Ramankutty, 2004). The HYDE database presents historical population and landuse patterns going back to the year 10,000BC and up to 2005AD. It was produced by combining historical population data from multiple sources.

A group of more than 30 research teams joined together to produce the Global Land Cover 2000 (GLC2000) landcover product (Bartholome & Belward, 2005). The GLC2000 product is a multi-class landcover product and urban is one of the classes included. The different teams brought regional expertise to modeling landcover in various

regions of the world. The product was created from data collected by the Vegetation-1 instrument on-board the SPOT-4 (Satellite Pour l'Observation de la Terre) satellite. In certain regions ancillary data such as Along-Track Scanning Radiometer (ATSR) thermal images and European Remotes Sensing (ERS) satellite radar images were used. Additionally, nighttime lights data were used to help delineate urban areas.

One of the earliest available global maps was Vector Map Level 0 (Potere & Schneider, 2007). It is a vector product produced at 1:1,000,000 scale by digitizing a large collection of maps and nautical charts. Although it has several shortcomings, such as not listing the date of the underlying source data and ignoring interior patches of non-urban land, it is considered a conservative estimate of urban land area and used as in input to several other products (Potere & Schneider, 2007).

In addition to these data products there have been several products made from only nighttime lights data that map urban area. Imhoff et al (1997b) describe a method for delineating urban areas with nighttime lights data by applying a percent detection frequency threshold to the data. The end product was a binary map of urban and non-urban land cover based on the determined threshold. This process was also attempted by Henderson et al (2003) who noted that the process of thresholding nighttime lights to define urban areas exaggerates the size. Despite this shortcoming the authors also suggest that the data could be calibrated in order to monitor growth of cities at comparable levels of development. Small et al (2005) further consider the use of nighttime lights alone to map urban areas. The authors found that there are several shortcomings in the data that make it difficult to find accurate urban extents from nighttime lights data alone. However, they note some possible methods for improving the process in the future, as

well as the new sensors (such as the Visible Infrared Imager Radiometer Suite - VIIRS) that will eventually alleviate some of these issues.

Another product made from nighttime lights, combined with Landscan, is a map of impervious surface area (ISA) (Elvidge et al., 2004a; Elvidge et al., 2007d). This product maps impervious surfaces globally at a grid resolution of 1km. It was generated by building a linear regression with nighttime lights and Landscan (ambient population) as the predictors. The National Land Cover Dataset (NLCD) impervious surface product for the United States was used to calibrate the model. The NLCD data were generated from Landsat scenes based on a complex decision tree analysis for the continental U.S. (Yang et al., 2003). There was a very large amount of effort involved in generating the 30m NLCD impervious surface product and no one has yet seen fit to undertake the same process globally. While the impervious surface product made from nighttime lights and Landscan is not a map of urban area in its strictest sense, as it aims to maps ISA in all areas not just urban areas, it is nonetheless a useful product in considering the impacts of humans and urbanization.

Potere & Schnieder (2007) compared a number of data sets that can be used for making an estimate of urban area. The data sets used included, VMAP0, GLC2000, HYDE, ISA from nighttime lights and Landscan, the urban landcover product described by Schneider et al (2003), and GRUMP. The authors tabulated the urban are estimated by each product in square kilometers (Table 1). They also calculated a total urban area based on the UN Population Divisions national level urban statistics and regional level urban population densities. These estimates show a wide range of differences overall, but less difference when the two products at the extremes are ignored.

Table 1: Estimated urban area from multiple remotely sensed products (Potere & Schneider 2007).

Product	Estimated Urban Area in Square Km
VMAP0	276,000
GLC2000	308,000
HYDE	532,000
ISA	572,000
MODIS, Nighttime Lights, Population, NLCD	727,000
GRUMP	3,524,000
Non-Spatial Estimate based on national level population data	500,000

Potere & Schnieder (2007) draw several important conclusions from their comparison of these urban maps. First, despite significant effort from a wide variety of organizations the products differ considerably. Second, differences exist in these products at the scale of regions, countries, and urban patches. The highest correlations between these products are in North America and the lowest in Asia. The authors note that these differences could be due to a number of factors including the timing of production, map resolution and class enumeration, as well as fundamental differences in the approach to urban land taken by the different groups responsible for these products. The authors also state that creating a workable definition of urban is not a trivial task.

To date a significant amount of effort has been put into creating global maps of urban extent. Despite these efforts there still remains a great deal of work to be done to improve these products and make them more useful to possible users. There is a need for more discussion on defining the terms urban and urbanization in the context of urban maps. More validation of the products is necessary to determine the accuracy. The data used in these products needs to be assessed and possible gaps in the necessary inputs identified. Also, there still remains room for refining the techniques used to produce these products.

More specifically to the research presented here is the pervasiveness of nighttime lights as an input to urban area products. “Artificial lighting is a unique indicator of human activity that can be measured from space” (Elvidge et al., 2007c). It seems clear that this product provides a unique and useful measure for use in urban mapping. However, there are shortcomings in the data (Elvidge et al., 2007a; Elvidge et al., 2001b; Elvidge et al., 2007c; Elvidge et al., 2007d; Henderson et al., 2003; Imhoff et al., 1997b; Small et al., 2005). These issues include spatial and spectral resolution, calibration (between years and satellites), geolocation accuracy assessment, and levels of quantization. The VIIRS onboard NASA's Suomi National Polar-orbiting Operational Environmental Satellite System Preparatory Project (NPP) spacecraft, will begin to address issues of calibration, spatial resolution, and levels of quantization (Small et al., 2005). The proposed Nightsat mission would address issues of calibration, spatial and spectral resolution, and levels of quantization (Elvidge et al., 2007a; Elvidge et al., 2007c).

Ecological Impacts of Light at Night

The ecological impacts of light at night are numerous (Longcore & Rich, 2004; Navara & Nelson, 2007; Pauley, 2004) and not always well understood. Nocturnal light emissions affect both humans and other species with impacts ranging from increased risk of disease to increases in infant mortality. Studies of this topic have been carried out for decades and recent discoveries have further highlighted the negative physiological, epidemiological, and ecological impacts of nighttime lighting.

Baker and Richardson (2006) discuss the impacts on male green frogs during breeding season, which call less often for mates when artificial lights are present.

Bertolotti and Salmon (2005), Karnad et al. (2009), Philibosian (1976), and Salmon and Witherington (1995) address some of the impacts and concerns of nighttime lights as they relate to sea turtles. In particular, sea turtle hatchlings are often disoriented by artificial lights after hatching and unable to find their way into the ocean leading to increased mortality. Moths and bats are also negatively impacted by artificial lights at night (Acharya & Fenton, 1999; Blake et al., 1994; Boldogh et al., 2007) with impacts ranging from increased ease of moth predation by bats, to slower rates of growth and birth, which can lead to the death of entire colonies of bats. It has been determined that certain spectrums of light disrupt the orientation and migration of certain species of birds (Wiltschko et al., 1993; Wiltschko & Wiltschko, 1999) as well.

Artificial nocturnal lighting also appears to have significant impacts on human health. Numerous studies have identified correlations that should raise concerns about artificial nocturnal light. A study of nighttime lights in Israel found a correlation with incidence of breast cancer in the female population (Kloog et al., 2008; Lee, 2008). Studies such as this one highlight the value of DMSP OLS data for observing and monitoring the impacts of nighttime lights on human health.

Pauley (2004) discusses evidence of a correlation between lights at night and increased incidences of breast and colorectal cancers in shift workers. He also reports on the results of experiments on rats that highlight increases in cancer cell growth rates in rats exposed to light at night. Additionally, this study identifies specific wavelengths in the visible spectrum that may be particularly harmful to humans at night. Pauley's conclusion includes a suggestion that lighting fixtures should be designed to include

shielding that would minimize the impacts of lights at night to the normal circadian rhythms in plants and animals.

Improving our understanding of nighttime light data from the DMSP OLS could offer great benefit to our understanding of physiological, epidemiological, and ecological impacts of lights at night. This data could also be valuable in observing current lighting uses. In particular, DMSP OLS nighttime lights data could be used to estimate the amount of energy lighting the night sky. Areas that could potentially benefit from the improved light fixture design suggested by Pauley (2004), as well as areas where energy costs are increased by excessive lighting, could be identified, highlighting locations where possible health and economic incentives of light shielding exist.

Shortcomings of OLS Data

One of the primary shortcomings of the OLS nighttime lights is the fact that there is no on-board calibration for the visible band. It is known that there are slight differences between the satellites at launch and that the optical throughput of the OLS declines over time. A second shortcoming is the fact that the lighting features from the OLS are substantially larger than the lights sources present of the ground. This appears to be largely due to the large overlap between adjacent OLS pixels. That is to say, individual light sources are detected in multiple OLS pixels. This research investigates and aims to address both of these shortcomings.

Research Questions

This research addresses several questions.

1. Can a portable lighting source be used to further our understanding of the DMSP OLS, specifically the minimum detection brightness?

2. Can a portable light source be used as an active target for assessing the geolocation accuracy of the DMSP OLS?

3. Can a portable lighting source be used as an active calibration device on the ground for inter-annual and inter-satellite calibration of the DMSP OLS?

4. Can a portable light be used to estimate the nightly energy expenditures around the globe on light that is wasted into the sky?

Objectives

The objectives are to explore:

1. the feasibility of using a portable lighting system for achieving light detections from the OLS sensors

2. the minimal detectable brightness for the OLS

3. the geolocation accuracy of the nighttime lights products as currently processed

4. the use of data from these collects to develop an inter-calibration of the digital numbers from different satellites

5. an estimate of the total watts expended on light emitted into the night sky

Research Overview

To answer question one (objectives one and two) a portable lighting source is required. There are numerous styles of lighting products available on the market today. It was decided that a high intensity discharge (HID) light source would be the best for this research. A portable lighting source, consisting of high pressure sodium lamps common on warehouses, parking lots, and roads, was deployed in remote locations (distant from other detectable lights), pointed straight upwards at the time of overpasses by the DMSP

OLS. Between 18 March 2009 and 1 April 2011 the portable light system was fielded on 27 separate nights. On 13 of those nights the usable data was collected resulting in 28 images from two satellites.

During the field tests the lights were turned on at least 45 minutes before the expected overpass time. The overpass time can be predicted to within a minute given the ephemeris available for the DMSP satellites. Pointing the lights directly at the sensor each night was considered, but ultimately it was decided that the omni-directional nature of the lights made this irrelevant. During each experiment the lights were pointed straight upward with a 22 inch aluminum reflector around the base.

Sunlight and moonlight can decrease the quality of DMSP OLS imagery when present. Between mid-September and mid-April the solar elevation and lunar illuminance are acceptable for carrying out these tests (figure 1). All tests were carried out on nights when the lunar illuminance was less than 0.0005 lux and the solar elevation was less than -12 degrees. Using the satellite observed brightness, the brightness of the lights on the ground, and the optical depth an estimate of the minimum detectable brightness was determined and a method for inter-calibration for use between satellites and years was defined.

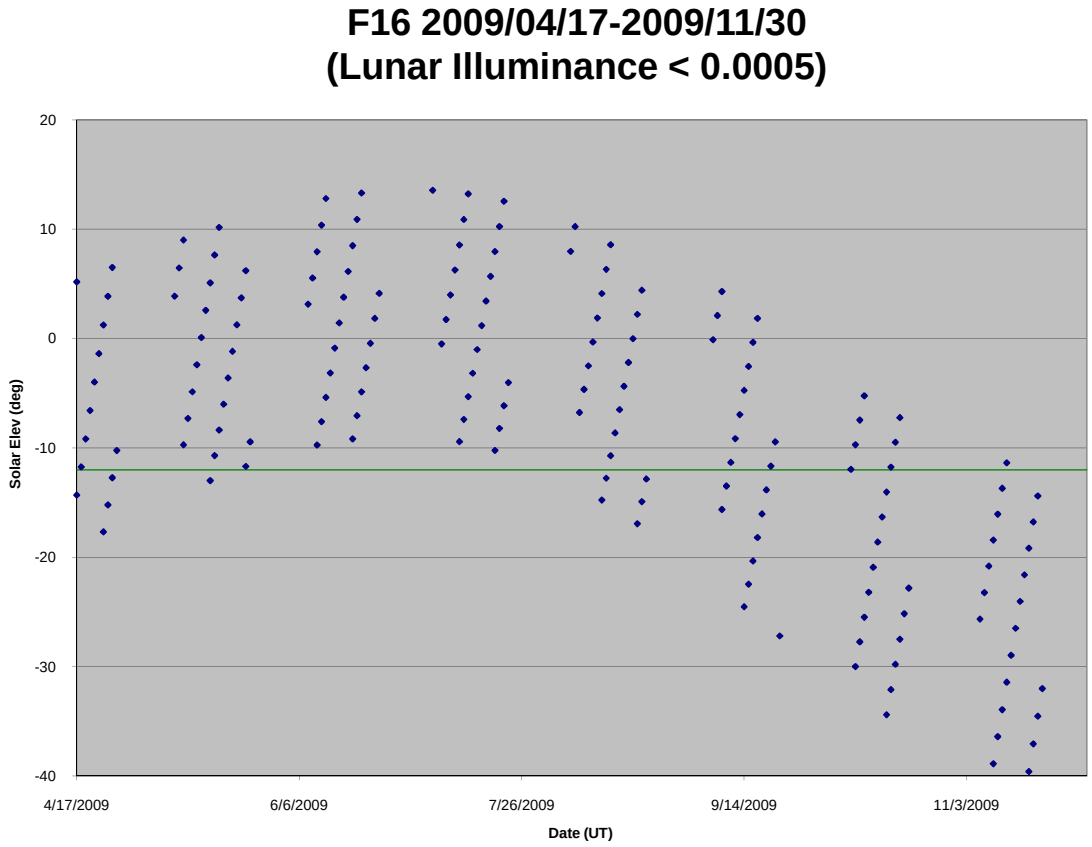

Figure 1: The solar elevation by night at the local time of satellite overpass, the green line marks -12 degrees solar elevation, only points below the green line are considered acceptable.

In order to address question two (objective three) GPS latitude, longitude and altitude data were collected for each of the field sites. The location of the light collected in the field was compared to the location of the light as observed by the satellite. The differences were identified for each experiment and later analyzed to quantify any shift (systematic or random) in the geolocation of the DMSP OLS data.

To address question three (objective four) the brightness of lights used during each field experiment was recorded. Once the imagery was collected data on the scan angle, gain, digital number (DN), satellite, and resolution was recorded. Using these

details it is possible to use linear regression to build a model to predict radiance based on brightness of lights. This is the basis for preparing inter-calibration models for the DMSP OLS.

Question four (objective five) can be answered by building upon the work to address the first three questions. Using the portable light and the inter-calibration process it is possible to convert radiance observed by the OLS into watts of energy used to produce that radiance. Using this conversion data on the watts expended each night on light emitted into the sky has been estimated and mapped.

Outcome and Impact

- Establish a hardware configuration and repeatable procedure for the collection of standardized light detections from the OLS.
- Development of an empirical calibration for estimating radiances from OLS digital numbers.
- By repeating the procedure over time we will be able to track the decline in optical throughput of the individual OLS sensors.
- A precise determination of the geolocation accuracy of the nightly OLS nighttime lights products.
- Estimate the watts expended per night around the globe on light emitted into the sky at night.
- Provide insight as to the detection limits of the DMSP OLS sensor.

Benefits

At this time there is no absolute method for inter-calibrating the data from different DMSP satellites with the OLS sensor on board. This research provides a methodology for inter-calibrating the data between different satellites. The sensors are

not only different between satellites, but can degrade over time. This means there is also a need to be able to inter-calibrate between years for the same satellite. This research also provides a method for inter-calibrating between years.

Additionally, assessment of the geolocation accuracy has been limited to isolated point sources of light such as offshore oil platforms. This project provides a new method for geolocation accuracy assessment. This additional method also has the benefit of flexibility and control of the isolated point source. A portable light can be used in multiple locations chosen by the researchers and users. This gives the ability to use a greater number of points in the accuracy assessments.

These methods could have future applications for other sensors. The VIIRS also has a visible band that could benefit from the methods this project endeavors to develop. This process could also be applied to the Nightsat mission (Elvidge et al., 2007a; Elvidge et al., 2007c). Both VIIRS and Nightsat have higher spectral resolution than the DMSP OLS and these will be accounted for in designing the final lighting configuration intended as an output from this research.

Chapter Two: It Used To Be Dark Here: Geolocation Calibration of the Defense Meteorological Satellite Program Operational Linescan System

Introduction

Nighttime satellite imagery is distinct as it observes emitted rather than reflected radiation. Data products derived from Defense Meteorological Satellite Program (DMSP) Operational Linescan System (OLS) nighttime satellite imagery are used for an increasing number of applications. The coarse spatial resolution of the DMSP OLS imagery presents some interesting challenges with respect to characterizing the positional accuracy of the images. This paper presents a methodology for characterizing the geo-location accuracy of the standard geo-referenced image products provided by the National Geophysical Data Center (NGDC). In short, we travelled to 'dark' places and lit them up with a portable light source that was detected by the DMSP OLS. We compared GPS coordinates taken at these 'dark' sites to the location of the 'new' light detected by the DMSP OLS.

The DMSP OLS was first launched in 1972. Each satellite is in a sun-synchronous near-polar orbit of 104 minutes at an altitude of 830km above the earth's surface. The sensor has a 3000km swath and provides global coverage two times per day. The DMSP satellites are flown in either a dawn-dusk or day-night orbit. The OLS has a thermal band which is sensitive to radiation from 10.0 – 13.4 um and a visible band sensitive to radiation from 0.58 – 0.91 um.

The DMSP OLS was designed to observe clouds, however, the use of the OLS's photo-multiplier tube (PMT) at night give the OLS a unique capability. During periods of low lunar illuminance and low cloud cover the OLS is able to observe nocturnal light emissions from the surface of the earth. This includes light emitted by cities, fires, gas flares, and heavily lit fishing boats, providing a way to observe the extent of human influence in ways that were not previously available on any other remote sensing platform.

The OLS collects data at a spatial resolution of 0.55km^2 ground-sample distance (GSD) known as fine resolution. However, these data are converted to smooth resolution of 2.7km^2 GSD by averaging a 5x5 grid of fine pixels for global coverage. A limited amount of higher resolution (fine) data is recorded and transmitted to the ground station based on requirements set by Air Force Weather Agency (AFWA). The instantaneous field of view (IFOV) of the fine resolution data, collected by the PMT, is 2.2km^2 at nadir and expands to 4.3km^2 at 800km from nadir. At 800km the PMT electron beam shifts to constrain the enlargement of pixels reducing the IFOV to 3km^2. At the edge of the swath (1500km from nadir) the IFOV is 5.4km^2. So the IFOV is significantly larger than the GSD. For the smooth resolution PMT data the IFOV at nadir is 5km^2 and at the edge of the swath is approximately 7km^2. More details on the OLS can be found at the NGDC website (http://www.ngdc.noaaa.gov/dmsp) and in publications by Elvidge et al (2001b; , 2004b) and Baugh et al (2010).

In 1992 the NGDC in Boulder, CO began a digital archive of the DMSP OLS data, prior to that the data were stored on film reels. NGDC provides the data in several forms ranging from raw orbits to geolocated annual composites. The annual composites

are made by collecting all the cloud-free data from the dark portion of the lunar cycle, thus avoiding the inclusion of moonlit clouds (Elvidge et al., 1999; Elvidge et al., 1997b; Elvidge et al., 2001b). These products have been found to overestimate the size of the lights on the ground (Small et al., 2005). Despite this shortcoming the nighttime lights data collected by the OLS has been used in a wide variety of studies. OLS nighttime lights data have been used for estimations of population and energy consumption (Elvidge et al., 1997c; Lo, 2001; Sutton, 1997; Sutton et al., 1997), mapping urban areas (Cova et al., 2004; Henderson et al., 2003; Imhoff et al., 1997b; Schneider et al., 2003; Small et al., 2005), estimation of forest area impacted by wild fires (Elvidge et al., 2001c), studies of net primary productivity and carbon modeling (Milesi et al., 2003; Milesi et al., 2005), estimating impervious surface area (Elvidge et al., 2004a; Elvidge et al., 2007d), modeling population density (Sutton et al., 1997; Sutton et al., 2003), estimating informal economies (Ghosh et al., 2009; Ghosh et al., 2010b; Ghosh et al., 2010c), and monitoring global gas flaring volumes (Elvidge et al., 2009c).

Assessment of positional accuracy is essential to understanding satellite imagery and improving the results of research relying on that imagery (Cuartero et al., 2010; Dolloff & Settergren, 2010; O'Hara et al., 2010; Qiao et al., 2010; Surazakov & Aizen, 2010). Given the breadth of applications a firmer understanding of the positional accuracy of the OLS is in order. Elvidge et al (2004b) examined the positional accuracy of the OLS. This study examined the characteristics of the OLS on board satellites F10, F12, F14, and F15. The OLS data were compared to locations of point sources of light extracted from Landsat ETM+ 15m panchromatic data. The smooth data was found to

have accuracies between 1.55 and 2.36km (less than the GSD of one smooth pixel) with satellite F14 having the best accuracy and satellite F10 the worst.

At present the two satellites flying in a day/night orbit (making them useful for the observation of nighttime lights) are F16 and F18. Neither of these satellites was in orbit at the time of the previous study. Additionally, rather than using Landsat data to extract locations we have devised a new methodology. Our research has found that it is possible to construct a portable light source capable of detection by the OLS. We present the details of this light source as well as methods for determining the positional accuracy of the OLS using such a light source.

Methods

Overview

A portable light capable of being observed by the DMSP OLS was designed. A commercially available high pressure sodium lamp was selected after evaluating multiple options. Three sites with no existing light sources were selected for use in field experiments. Each site was measured with a GPS and the points were differentially corrected. During each field experiment, the lights were deployed and turned on prior to the predicted overpass of the satellite. The observed location of the light by the OLS was compared with the known location measured by GPS to perform a positional accuracy assessment.

Light Design

We set out with a need to design a portable light source that could be detected by the DMSP OLS. There are a wide variety of commercial lighting products available to choose from and some empirical studies were required to settle on an appropriate design.

Many factors had to be considered including lumens/watts ratio, the spectral characteristics of the light source, and the ability to easily transport of the light source from one sight to another.

The field experiments were started using standard off the shelf halogen work lights (available at stores such as Home Depot or Lowes). Several field experiments proved that the halogen work lights were not bright enough to be detected by the OLS in quantities that could be easily powered in the field. In order to power enough of these lights to achieve detection would have required more power than could be easily transported. This is due to the halogen work lights low lumens/watts ratio.

This was followed by evaluating concentrated three million candle power hand held spotlights. Unlike the previously mentioned light sources measured in lumens these spot lights were measured in candle power. Lumens are a measure of the total visible light emitted by a source, while candle power (or candela) is a measure of the total visible light emitted by a source in a particular direction. These spotlights are designed to focus a beam of light on a specific location, hence the term spot light. The lights previously, mentioned and the lights eventually chosen for this study are omni-directional and their brightness is measured in lumens. The hand held spotlights are believed to have been bright enough if pointed directly at the sensor, but even with accurate predictions of the sensor overpass it proved to be difficult to document proper or improper aiming on any given night.

This led to evaluating high intensity discharge (HID) lighting options. The current configuration relies on high pressure sodium lamps common in applications such as

warehouse lighting. These lamps are available in varying sizes including 250 watts and 1000Ws, both used in these experiments.

These high pressure sodium lamps emit most of their energy in the orange to red portion of the visible spectrum from 560 – 740 um (figure 2). The emitted energy fits well within the optical window of the atmosphere. Additionally, these wavelengths are less prone to Rayleigh scattering than the shorter wavelengths produced by other high intensity discharge lighting options such as metal halide lamps. In addition high pressure sodium lamps have a higher ratio of lumens/watts than metal halide lamps. Also, the peak emissions from the high pressure sodium lamps are within the peak response of the OLS sensor's spectral response curve (figure 3). Elvidge et al (2010) describe the spectral signatures of a variety of lighting types (including high pressure sodium) in an effort to document the optimal spectral bands to identify different lighting types.

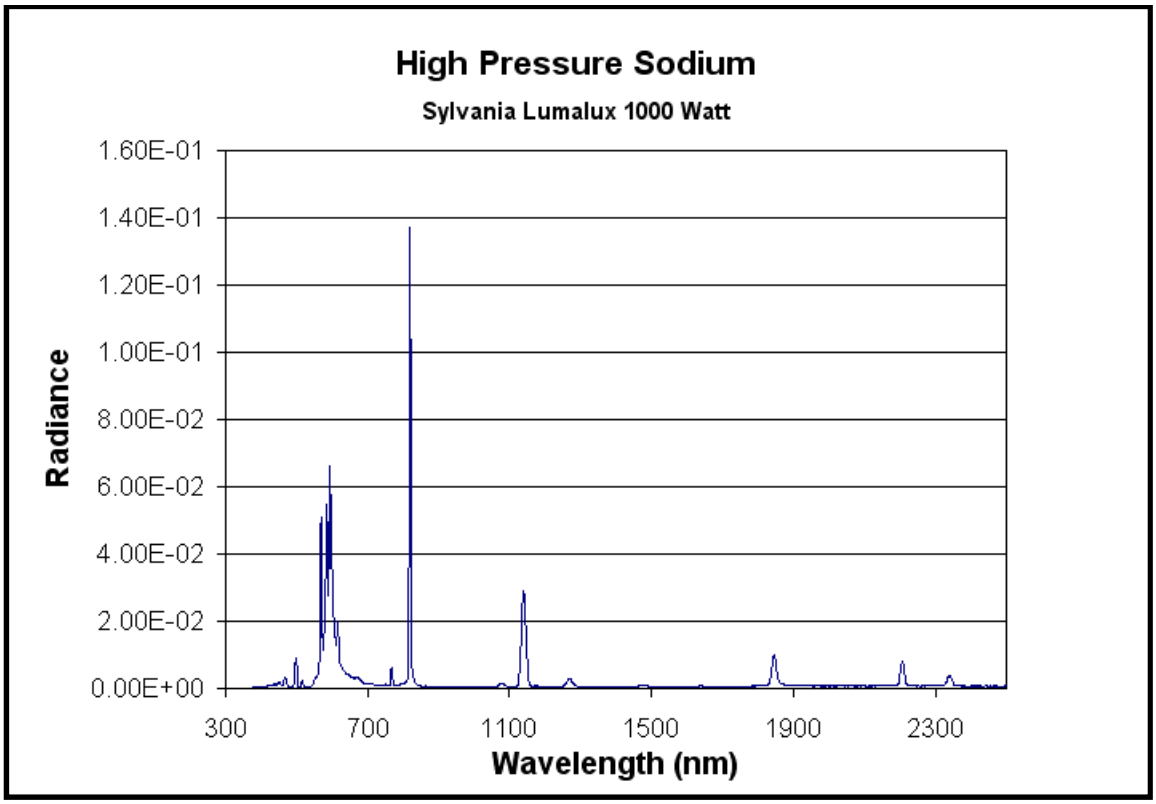

Figure 2: A Sylvania Lumalux 1000W high pressure sodium light bulbs spectral signature measured by an ASD spectrometer.

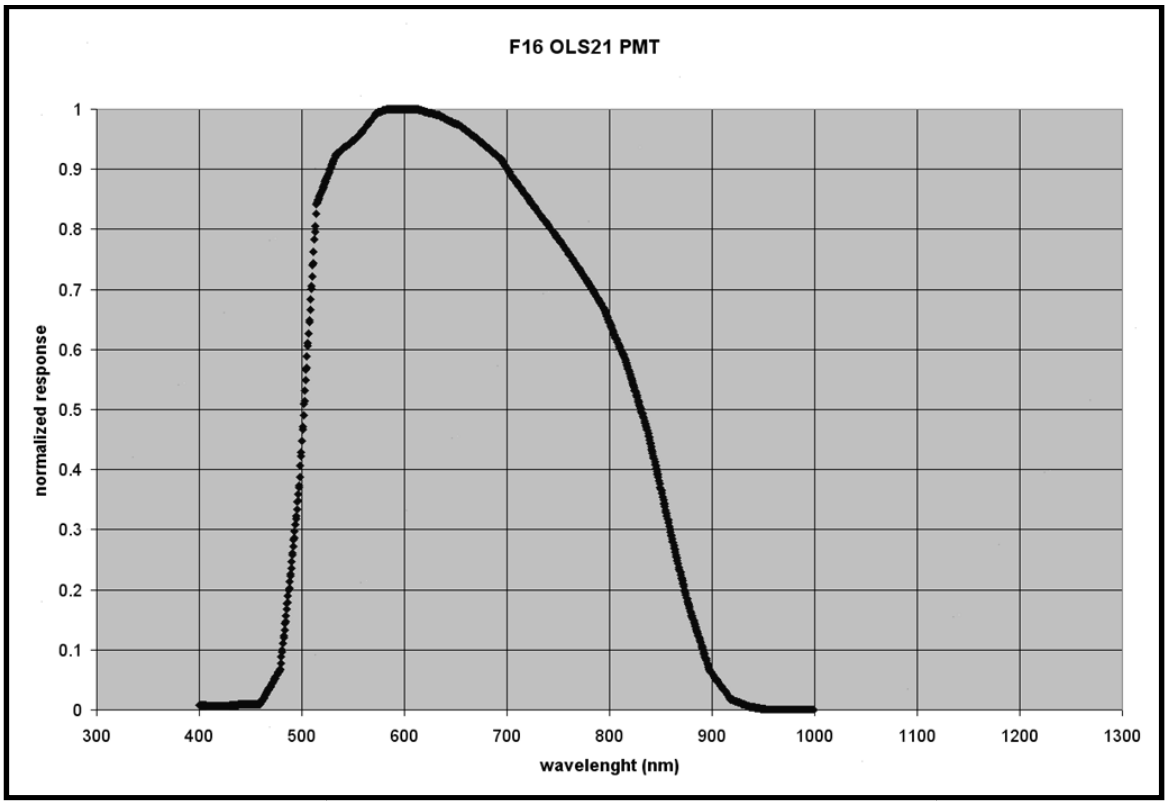

Figure 3: The spectral response of the DMSP OLS from satellite F16, measured pre-flight.

The high pressure sodium lights were easily purchased from vendors online. The 1000W lamps emit approximately 140,000 lumens and the 250 watt lamps emit approximately 35,000 lumens. For reference, the average 100 watt incandescent lamp emits approximately 1500 lumens. Once the lights were purchased wooden frames were designed and built to hold the light pointing upwards as they are designed to hang from a ceiling and point down. The frames hold the capacitor, igniter, ballast, and socket for each lamp and are open on top to allow for the attachment of a 22-inch (55.88cm) aluminum reflector and the lamps (figure 4). A total of eight 1000W high pressure sodium lamps and six 250 watt high pressure sodium lamps, the necessary frames for housing the fixture, and two 6000 watt gas generators fit on a 6-foot x 10-foot (1.83m x

3.05m) utility trailer (figure 5). Each 6000 watt generator can power up to four 1000W lamps at a time. This allowed for as many as eight 1000W lamps (approximately 1,120,000 lumens) or as little as one 250 watt lamp (approximately 35,000 lumens) at a time.

Figure 4: A 1000W high pressure sodium lamp with a 22 inch aluminum reflector.

Figure 5: Seven (1000W) high pressure sodium lights in the utility trailer and the two generators used to power the lights in the field.

Site Selection

Selecting the sites for these experiments involved several important factors. The requirements included accessibility, permission from land owners/managers, no other light sources or light pollution from nearby light sources, and accessibility to a truck and trailer throughout the year. Finding suitable locations that met all of these requirements was difficult. The identified sites that met the requirements range from approximately two to seven hours drive from the storage location of the lights.

One of the key factors in site selection was permission from the land managers of each location. Conducting the experiments at all sites were cleared with the relevant parties and local authorities were notified of every experiment prior to our arrival. This

was important especially because the lights were visible from roads up to five miles away and have an orange glow similar to that of a wild fire. Despite these efforts there were still occasions when concerned passersby visited the site during an experiment to see why a light had appeared where there normally wasn't one.

All sites were required to be completely dark, meaning no other light sources in the vicinity or light pollution from neighboring light sources. Each site was visited and GPS coordinates were gathered and differentially corrected. These points were overlaid on DMSP OLS annual composites to determine if the site was completely dark. Only sites with a DN value of zero in the annual composites were considered. Additionally, the sites had to be accessible. The lights and required power were transported in a utility trailer. Each site needed to be accessible to a truck pulling the trailer.

The DMSP orbit prohibits the collection of data with a clear view of sites in our area of interest during the summer (approximately mid-May to early September) because the sun sets too late. This meant that we conducted these field experiments in the winter and weather was an important factor in site selection. A site that was covered in more than one foot of snow for most of the winter was not considered accessible. Additionally, sites with consistent and predictable weather were considered more desirable than those with unpredictable weather, given that clouds can obscure the view of the portable light and make the data unusable. A site near the peak of Mt. Evans was examined on several occasions and was very desirable as it was close to the location the lights were stored, on property controlled by the University of Denver, and dark. However, it was found that predicting the weather there was too difficult to be worthwhile. For example, on one night with a prediction of clear skies it started snowing 30 minutes before the satellite

was to make an observation of the site. On the other hands sites such as the Santa Fe National Forest proved to be very stable based on weather predictions allowing for a higher percentage of the visits there to yield usable data.

Multiple sites were chosen to control for systematic versus non-systematic shifts in the geolocation. Based on the criteria a total of three sites were chosen, two in Colorado and one in New Mexico. The sites were the Pawnee National Grasslands in northeast Colorado, the Karval State Wildlife Area in southeast Colorado, and the Santa Fe National Forest in Rowe, New Mexico (figure 6). Each of these sites met all the criteria determined for a suitable site and were visited on multiple occasions.

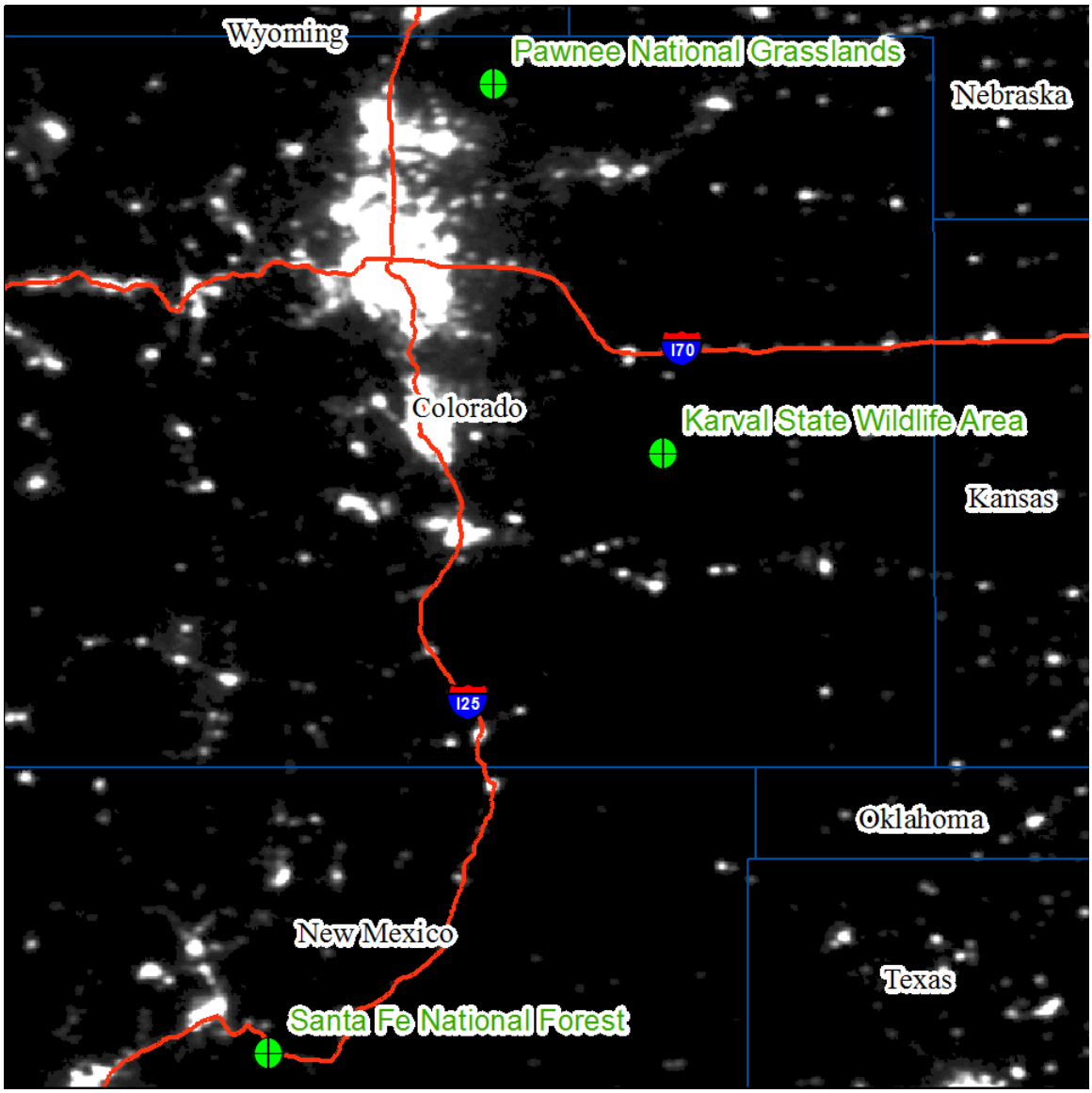

Figure 6: Map of the three field sites in Colorado and New Mexico with a nighttime lights annual composite from satellite F16 for the year 2009 as the background.

Field Experiments

Using the ephemeris available to the NGDC for the DMSP the time of observation at each site was predicted for each season (September to May) along with other relevant details such as scan angle, lunar illuminance, and solar elevation. To avoid sun light or moon light in the imagery only nights when the solar elevation was less than

-12 degrees and lunar illuminance was less than 0.0005 lux were considered for inclusion in the study. Using this information, nights when the lunar illuminance and solar elevation were within acceptable ranges for clear observations could be determined. Predictions of the observation time at each site were then calculated out in four week intervals as time went by to get more accurate times. In the experiments, the predicted time of observation was always within seconds of the actual time of observation. Following this the weather predictions at each site were monitored for times when there was a prediction of clear skies and the lunar illuminance and solar elevation were within acceptable ranges. Based on this information the nights to conduct the experiments were chosen.

When conducting the experiments the lights were set up well in advance of the predicted observation time. The trailer was always placed in the same location that the GPS coordinates were measured for each site. High pressure sodium lamps do not achieve their peak intensity when first turned on. To ensure that the lights achieved their peak brightness they were turned on 45 – 60 minutes prior to the predicted observation time. The lights were then left on until after the predicted observation times had passed. Different numbers of lights were used on different nights in order to be able to examine changes in observed brightness for use in other studies.

The possibility that pointing the lights at the sensor would achieve better results was considered. It is possible to calculate the direction and angle at which the sensor would observe the site on each night. However, our initial tests showed that with these lights there was no significant difference between pointing the light at the sensor and just pointing it straight up into the sky. This is likely because the 22 inch aluminum reflector,

although it helps direct the light upwards, does not have enough of a concentrating effect to achieve any difference from pointing directly at the OLS sensor.

The OLS sensor typically observes a light source in more than one pixel as the ground footprint of the pixels overlap. These characteristics are further described by Elvidge et al (2004b) and the portable light source was observed in multiple pixels in the imagery on any given night. After returning to the lab this fact was clearly observed in the imagery of the portable light source. In the fine imagery the lights often registered in upwards of 10 pixels and in the smooth imagery commonly registered in 4 – 8 pixels, depending on the number of lights used on a given night.

There is never a single pixel that represents the light in the imagery collected, thus on each successful observation all the pixels in which the light source were detected were outlined in the imagery. The resulting polygon shapefile represented all the pixels in which the light was observed on each night. In order to indentify a single latitude and longitude representing the location of the light in the imagery the centroid of each polygon was calculated using the "Feature to Point" tool in ArcGIS®. The distance and bearing from the GPS latitude and longitude for the site to the observed latitude and longitude from the imagery was calculated using the Spherical Law of Cosines. The equation used for the Spherical Law of Cosines distance is shown in equation 1.

$$Distance = ACOS(SIN(lat1)*SIN(lat2)+COS(lat1)*COS(lat2)*COS(lon2-lon1))*6371$$

Equation 1: Spherical Law of Cosines.

In addition to the distance from the GPS point, the bearing from the GPS point to the observed location was calculated using the following equation 2.

$$\text{Bearing} = \text{ATAN2}(\text{COS}(\text{lat1})*\text{SIN}(\text{lat2})-\text{SIN}(\text{lat1})*\text{COS}(\text{lat2})*\text{COS}(\text{lon2-lon1}), \text{SIN}(\text{lon2-lon1})*\text{COS}(\text{lat2}))$$

Equation 2: Calculation of bearing from point a to point b.

Results and Discussion

The results are reported in table 2 and show the mean and median distance in kilometers and the mean and median bearing in degrees (reported between -180° and 180° where north is 0°). The results are reported for all data points, separated by satellite, separated by resolution, and separated by both satellite and resolution. The overall mean and median are based on 28 points. Of the 28 points 18 were collected at the Karval State Wildlife Area site, 8 were collected at the Santa Fe National Forest site, and 2 were collected at the Pawnee National Grasslands site. Nineteen of the 28 points were collected by satellite F18 and 9 were collected by satellite F16. The smooth resolution data collected consisted of 18 points and the fine data collected consisted of 10 points. The geographic spread for the points at each site relative to the GPS measured location of the light source can be seen in figure 7.

Table 2: The mean/median distance and mean/median bearing between the GPS measured site locations and the observed locations in the imagery aggregated by satellite and sensor resolution.

	Mean Distance (km)	Mean Bearing (-180° to 180°)	Median Distance (km)	Median Bearing (-180° to 180°)
Overall	2.90	-0.05	2.81	-0.05
F16	2.49	-0.05	2.72	-0.03
F18	2.88	-0.06	2.75	-0.07
OLS	2.97	-0.10	2.86	-0.11
OLF	2.46	0.01	2.45	0.03
F16OLS	2.59	-0.06	2.85	-0.02
F18OLS	3.13	-0.12	2.94	-0.14
F16OLF	2.32	-0.04	2.58	-0.04
F18OLF	2.51	0.03	2.45	0.05

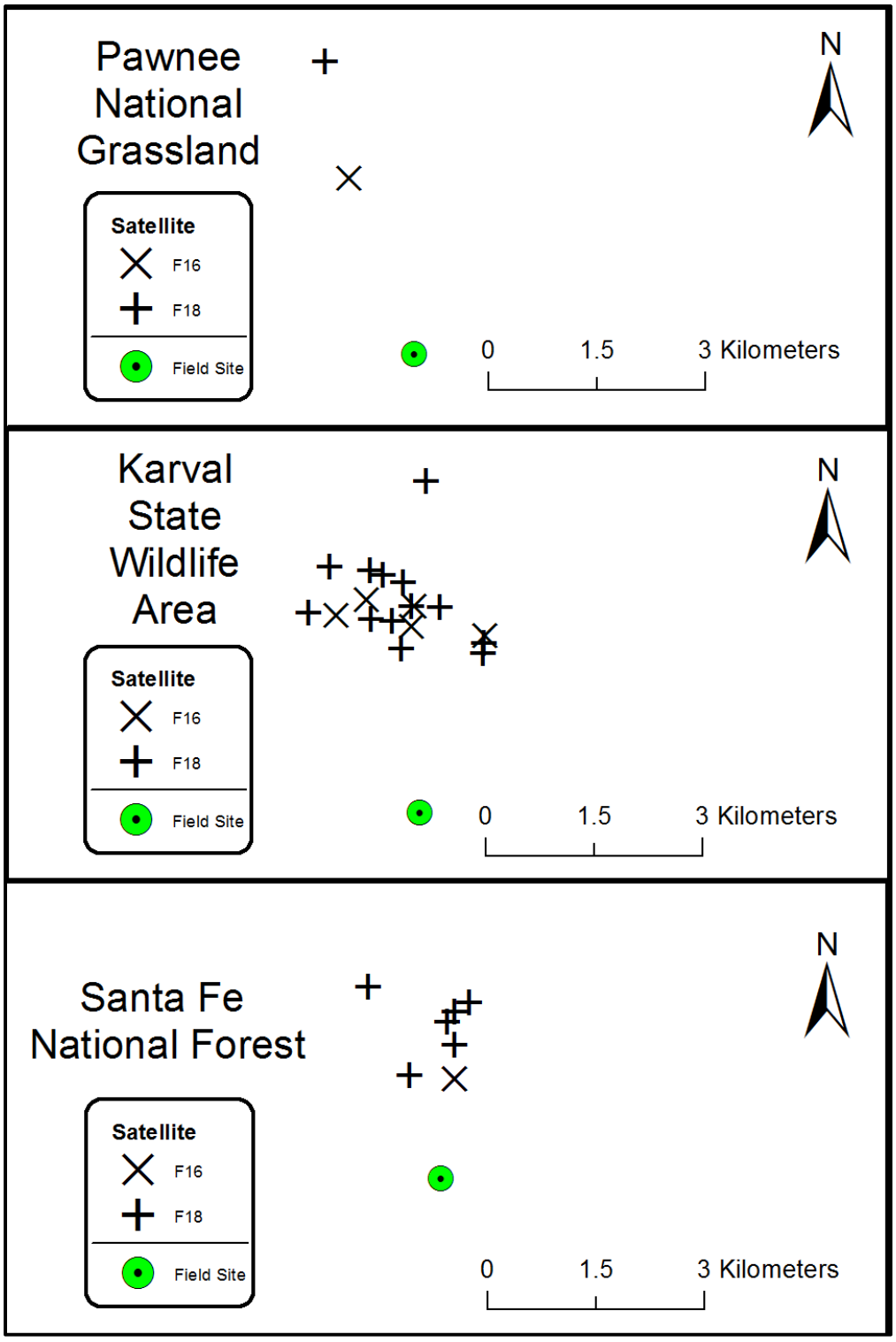

Figure 7: Maps of GPS measured location at field sites and all the satellite observed points at each site.

The overall mean for the distance between the measured GPS location and the observed location in the imagery was 2.90km and the median was 2.81km. For all the data points collected the mean and median bearing is the same at -0.05 degrees. The mean distance is just slightly larger, by 0.2km, than one smooth pixel and just over five times larger than one fine pixel. Additionally, the shift appears to be systematic in nature with the shift being about one smooth pixel almost directly to the North in all cases. Since the shift appears to be systematic it should be easy to correct by shifting the data by approximately one smooth pixel to the south. Applying a simple shift would be beneficial in studies merging or comparing this data with other data sets.

The means and medians grouped by satellite in table 2 show that F16 (9 data points) has a slightly lower mean than F18 (19 data points), while the medians are nearly identical. This is due to two points collected by F18 with distances of 4.582km and 5.436km from the measured GPS point. The maximum distance from the GPS for any F16 points was 3.314km. Anecdotal observations of the data by regular users suggest these slightly higher offsets can be seen in data from F16 as well. It is possible that with a larger sample size similar distances would have been seen with F16 bringing the means closer together. For F16 the mean bearing from the GPS point to the observer location is -0.05 degrees and the median is -0.03 degrees. Satellite F18 has a mean bearing of -0.06 and a median bearing of -0.07.

Looking at the data grouped by pixel resolution the smooth data (18 data points) has a higher mean and median distance from the measured GPS point than the fine (10 data points) data (table 2). The smooth data is collected by averaging a 5x5 grid of fine pixels taking the pixel resolution from 0.55km^2 to 2.7km^2. This process may account for

the slight increase in the offset for the smooth data. The smooth data has a mean bearing of -0.10 degrees and a median of -0.11 degrees from the GPS point to the observed location. The fine data has a mean bearing of 0.01 degrees and a media of 0.03 degrees.

When broken out by both satellite and resolution the F16 smooth (6 data points) data has a lower mean and median of 2.59km and 2.85km, respectively, than the F18 smooth (12 data points) data. These lower distances are likely due to the reasons discussed when examining F16 vs. F18 as the two data points with higher offsets were in the smooth data. The F18 smooth has a mean of 3.13km and a median of 2.94km. The F16 fine (3 data points) data has a lower mean at 2.32km, but a higher median at 2.58km, than the F18 fine (7 data points) data. The F18 fine data has a mean of 2.51km and a median of 2.45km. Measured from the measured GPS location to the observed location the F16 smooth data has a mean bearing of -0.06 degrees and a median bearing of -0.02 degrees. The mean bearing of the F18 smooth data is -0.12 degrees and the median bearing is -0.14 degrees. For the F16 fine data the mean bearing is -0.04 degrees, while the median bearing is -0.04 degrees. Finally, for the F18 fine data the mean bearing is 0.03 degrees, and the median bearing is 0.05 degrees.

Table 3 shows the mean and median distance in kilometers and the mean and median bearing in degrees (reported between -180° and 180°) grouped by site. There were 18 data points for the Karval State Wildlife Area, eight data points for the Santa Fe National Forest, and two data points for the Pawnee National Grasslands. Since there are only two points at the Pawnee National Grasslands site median is not reported. For each site the mean and median are very close if not identical. The Santa Fe National Forest had the lowest mean and median distance, while the Pawnee National Grasslands had the

highest mean distance. If more points had been collected at the Pawnee National Grasslands site, it would likely have had a lower mean similar to the other sites. The Karval State Wildlife Area has the most points and its mean falls between the other two sites. The mean and median bearings are very close together with a range across 0.36°. These results suggest that the distance and bearing are very similar at different geographic sites and it is expected that increased data points would bring these values even closer together. In fact none of the differences between offset distances and bearings between locations and satellites are significantly different on a statistical basis. Future research would benefit from collecting more points at the Santa Fe National Forest and Pawnee National Grasslands sites to confirm that a higher number of data points bring the means closer together across sites.

Table 3: The mean/median distance and mean/median bearing between the GPS measured site locations and the observed locations in the imagery aggregated by site.

	Mean Distance (km)	**Mean Bearing (-180°to 180°)**	**Median Distance (km)**	**Median Bearing (-180° to 180°)**
Karval State Wildlife Area	2.95	-0.06	2.85	-0.06
Santa Fe National Forest	1.97	0.00	2.01	0.08
Pawnee National Grasslands	4.37	-0.28	N/A	-0.28

It was hypothesized that the scan angle of the sensor at the time of collection might have had an impact on both the distance and bearing of the observed location from the measured GPS location. This hypothesis was tested by plotting smooth and fine data

distance and bearing were against the sample, which reflects scan angle, to examine this possibility. Figure 8 shows distance vs. scan angle for the smooth data points. The R^2 is 0.02 showing no relationship between distance and scan angle for the smooth data. Figure 9 displays the distance vs. scan angle for the fine data points. The R^2 of 0.08 shows no relationship between distance and scan angle for fine data either. Figure 10 charts bearing vs. scan angle for the smooth data points. The R^2 is 0.09 which means there is no relationship between bearing and scan angle for the smooth data. Figure 11 shows bearing vs. scan angle for the fine data points. The R^2 of 0.01 again demonstrates there is no relationship between bearing and scan angle for the fine data. Overall there is no relationship between distances or bearing, from the measured GPS point, and scan angle.

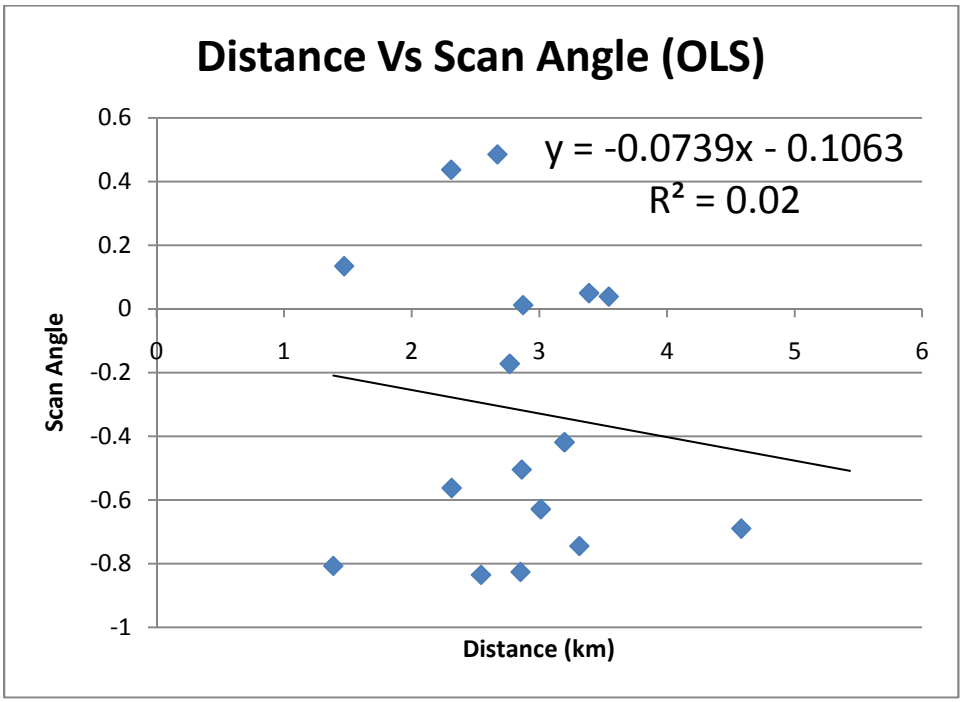

Figure 8: Graph of distance vs. scan angle for the OLS data.

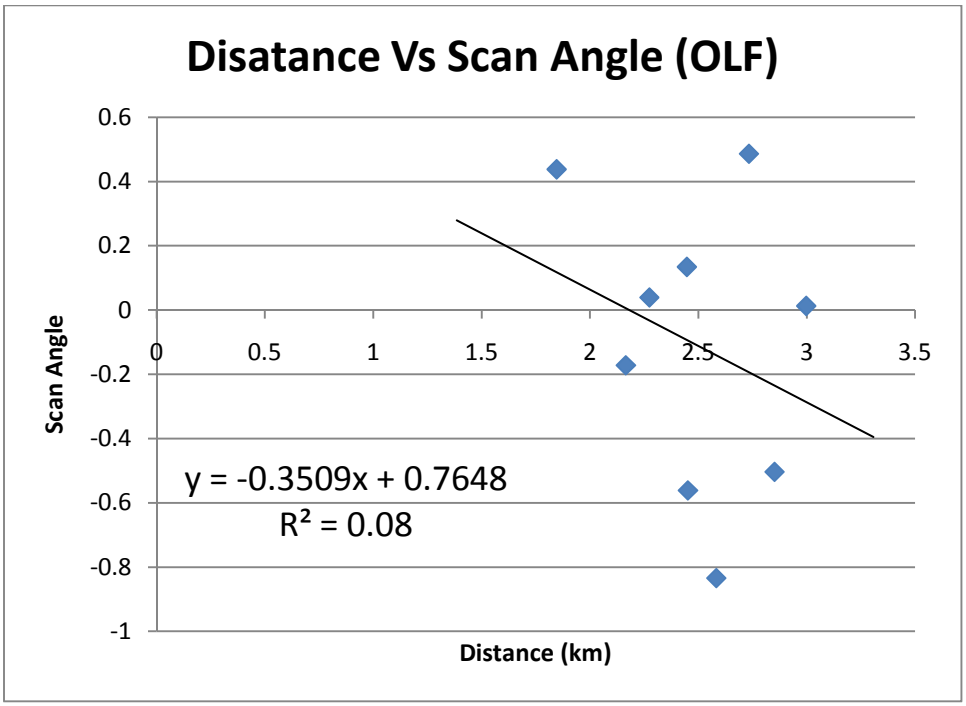

Figure 9: Graph of distance vs. scan angle for the OLF data.

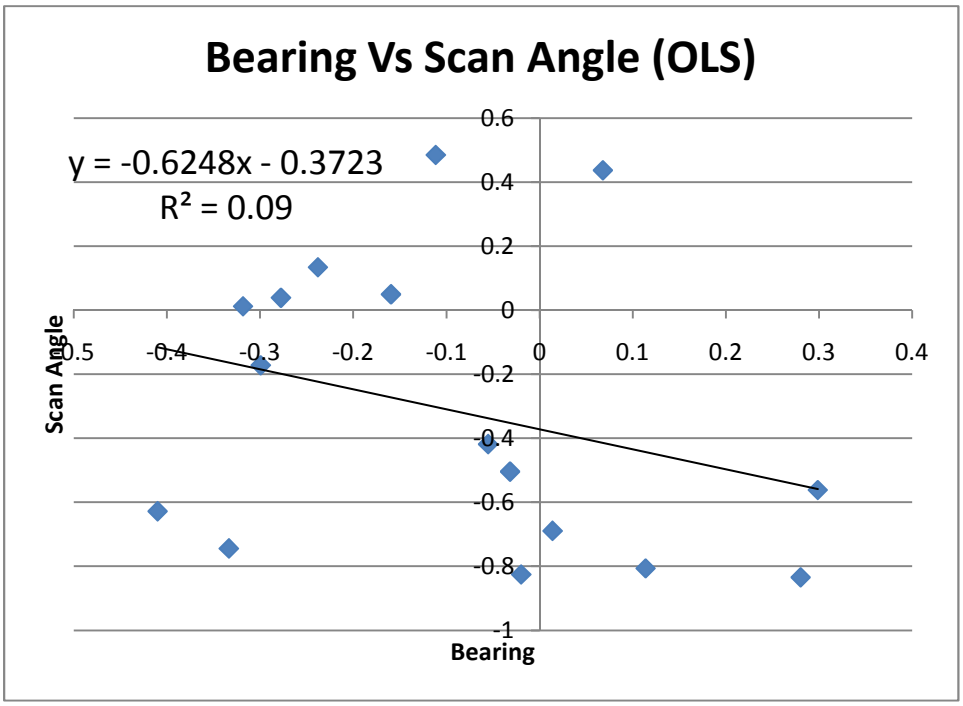

Figure 10: Graph of bearing vs. scan angle for the OLS data.

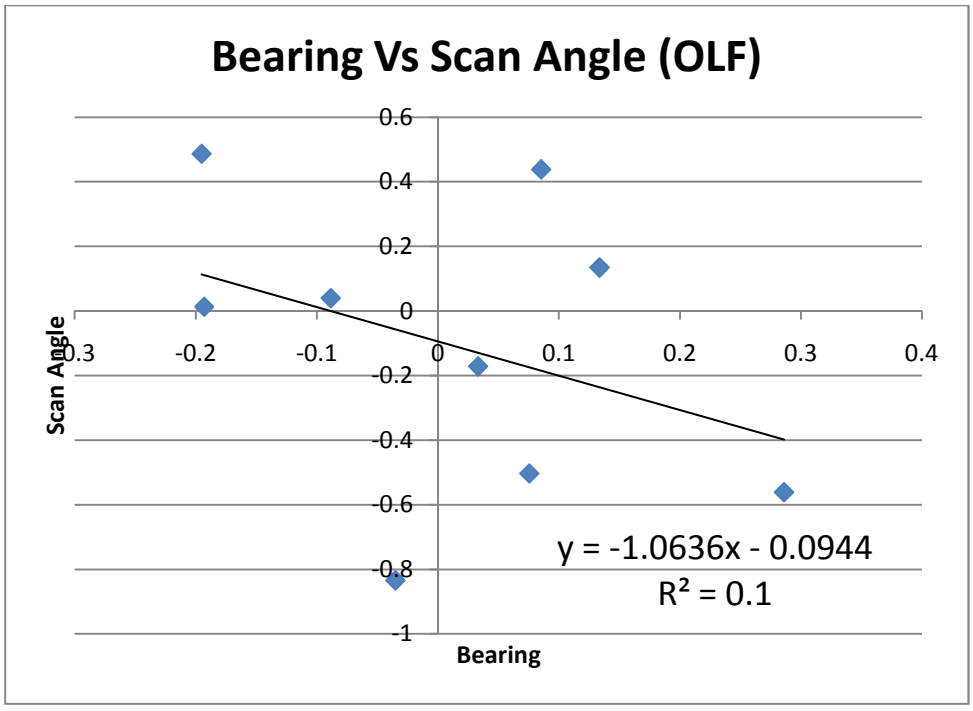

Figure 11: Graph of distance vs. scan angle for the OLF data.

Conclusion

A portable lighting system capable of detection by the DMSP OLS was designed and built. Three completely dark locations where the light could be setup were selected and GPS measurements of the locations were collected. Using the lights and these dark locations a repeatable process for measuring the location of the portable light and comparing it to the observed location in the DMSP OLS imagery was defined. Between 18 March 2009 and 1 April 2011 the portable light system was taken to these sights on 27 separate nights. On 13 of those nights the usable data points with no cloud cover were collected. The other 14 nights had cloud cover that obscured the light or the quantity of lights used was too dim to be observed. On the 13 nights when successful data points were observed a total of 28 images were collected. It was possible to collect multiple

images in one night as there were two satellites (F16 and F18) in orbit, on some nights a satellite would observe the light twice, and on certain nights both smooth and fine data were collected.

The mean distance between the measured GPS points of where the lights were setup and the observed locations of the light in the imagery was 2.9km and the median was 2.81km. The mean bearing measured from the GPS point to the observed location was -0.05° (measured between -180° and 180°) and the median was also -0.05°.This is just over a one smooth pixel shift to the north and a five fine pixel shift to the north. This shift appears to be systematic in nature and the fact that it is essentially the same for both satellites suggests the cause of the error is common to both satellites.

The data were collected at multiple sites in part to confirm either a random or systematic shift. Across the sites the bearing was in roughly the same direction ranging across 0.36°. The distances had a higher range across sites at 2.4km, however, two of the site had far fewer images collected. The site with 18 images was in line with the overall average with a mean distance of 2.95km between the GPS measured location of the light and the observed location in the imagery. It is expected that increasing the number of collections at the other sites, which had 8 images and 2 images, would bring them more in line with the overall average. Future research should include positioning the portable lighting system described here to determine if the systematic shift identified in this study is similar around the world. The results of this study suggest that the data products should be shifted by on smooth pixel to the south to correct for the geolocation offset identified.

Chapter Three: Aladdin's Magic Lamp: Active Target Calibration of the DMSP OLS

Introduction

Nighttime imagery of the earth captures many anthropogenically generated light emissions. Some from wildfires (Chand et al., 2006; Chand et al., 2007; Cova et al., 2004; Elvidge et al., 1998; Elvidge et al., 2001a; Elvidge et al., 2001c; McNamara et al., 2002), some from squid fishing squid (Elvidge et al., 2009a; Maxwell et al., 2004; Nagatani, 2010), some from the flaring of excess natural gas (Elvidge et al., 2007b; Elvidge et al., 2009c); however, the dominant signal in most nocturnal imagery is lights illuminating human settlements(Elvidge et al., 2001b). A fundamental question that motivated this work was: "*How many 100 watt incandescent light bulbs would it take in one location to be seen by the Defense Meteorological Satellite Program Operational Linescan System (DMSP OLS) sensor*?" We have noted that isolated truck stops along highways are visible in the imagery, while the cores of cities like Las Vegas, Nevada saturate the sensor. This research informs several questions with respect to the linking of the digital numbers (DNs) in a nighttime satellite image to the light energy emitted on the ground: 1) How to perform inter-calibration of different satellite platforms (the DMSP OLS has a series of independent satellites often operating simultaneously, in this study we used satellites F16 and F18)?; 2) How to perform inter-temporal adjustment of data to compensate for sensor degradation that takes place during the life cycle of the satellite.

There are many challenges associated with answering our fundamental question: 1) Background noise (Elvidge et al., 1997b), 2) gain variability of the OLS, 3) Optical depth to the sensor, 4) Degradation of the sensor over time, 5) Spatial resolution of the data (the DMSP OLS collects in two modes knows as “smooth” and “fine”), and 6) Overglow (a point source of light produces signal in multiple contiguous pixels in the imagery)(Small et al., 2005). Dark areas in the DMSP OLS imagery have DN values typically ranging from 0 - 5, this is the variability of background noise. An algorithm on board the sensor adjusts the gain in flight based on environmental conditions at the time between a pre-defined min and max. These adjustments are in response to changes in solar energy, lunar illuminance, and seasonal variability of day-night conditions. In accordance with original design goals, the gain is adjusted to optimize cloud observation rather than city lights. A fixed location on the ground will be observed at different scan angles on different nights due to variability in the orbital path of the satellite. Once outside the protection of the earth’s atmosphere the sensor is exposed to an array of radiation that leads to sensor degradation over time. The data are collected at a resolution of 0.6 km (known as ‘fine’ data) and this data is averaged in a 5x5 grid to create a 2.7 km pixel (known as ‘smooth’ data). The Air Force Weather Agency (AFWA) controls collections of fine data which is limited in nightly volume while smooth data is collected globally each night. The extent of the ground footprint of the OLS is larger than the spatial extent of the pixels in the imagery (this discrepancy increases with scan angle) (Elvidge et al., 2004b). This means that the energy represented by a pixel actually comes from a spatial area larger than that pixel and this effect is known as ‘overglow’.

Earlier attempts at dealing with sensor degradation pertaining to comparisons between satellite platforms and inter-temporal comparisons using the same satellite platform have been demonstrated. For example, Elvidge et. al. (Elvidge et al., 2009c) used the assumption of a stable region (Sicily, Italy) with no change over time to compensate for sensor degradation over time and between satellite platforms. Witmer and O'Loughlin (2011) also selected a set of cities determined to be stable over time to develop normalization functions for temporal inter-calibration. These methods improve the validity of change detection studies using inter-temporal and inter-satellite observations; however, they are plagued by the shortcoming of the assumption of 'stability'. Here we explore a method that improves upon the existing approaches to dealing with inter-temporal and inter-satellite comparisons.

Development of a methodology for identifying changes in the spectral sensitivity of the DMSP OLS will improve the validity of studies that examine differences over time in nocturnal images of the earth. Such studies include: Monitoring gas flaring emissions gas (Elvidge et al., 2007b; Elvidge et al., 2009c), mapping and monitoring CO_2 emissions (Doll et al., 2000; Ghosh et al., 2010a; Prasad et al., 2002), detecting the effects of war on human migration patterns (Witmer & O'Loughlin, 2011), mapping and monitoring economic growth and decline as sub-national levels (Elvidge et al., 2009b; Ghosh et al., 2010b; Ghosh et al., 2010c), mapping and monitoring changing patterns of human settlement (Cova et al., 2004; Elvidge et al., 2004c; Elvidge et al., 2007d; Henderson et al., 2003; Imhoff et al., 1997a; Imhoff et al., 1997b; Lo, 2001, , 2002; Potere & Schneider, 2007; Small et al., 2005), and population modeling (Lo, 2001; Sutton et al., 2003).

Data and Methods

Overview

A portable light, observable by the DMSP OLS, was fielded on 27 nights at sites with no existing light sources. The brightness of the lamps used on each night was recorded. DMSP OLS data for each night was collected and converted to radiance. Using linear regression, a model to predict radiance was developed. Additionally, varying amounts of light were used on different nights and an estimate of the minimum detectable brightness was defined.

Portable Light Design

A portable lighting source capable of being observed by the DMSP OLS was built to carry out this study. A number of options were explored, including off the shelf halogen construction lights and off the shelf spot lights. Based on the characteristics of the available lighting types a portable lighting source was designed using commercially available lighting products. High pressure sodium lights, commonly used in warehouses, were chosen for a variety of reasons. High pressure sodium lamps have a very high lumens to watts ratio, so more energy is converted to light vs. wasted as heat than in common household lamps. Additionally, the spectral emissions from high pressure sodium lamps are highest in the red/orange portion of the visible spectrum (figure 2). There is a low amount of Rayleigh scattering due to the red/orange character of these lamps allowing more energy to reach the sensor. The red/orange peak also coincides with the peak of the OLS pre-flight spectral response (figure 3).

The high pressure sodium lamps require a ballast, capacitor, and igniter to start the lamp and to regulate the current once the lamp is ignited. For these experiments

250W lamps and 1000W lamps were acquired. For the 1000W lamps the associated ballast, capacitor, and igniter weigh approximately 23kg each and are designed to hang from a ceiling. In order to direct the light towards the space borne sensor several portable housings were constructed to hold the ballast, capacitor, igniter, and socket housing with the bulb pointed skyward. A 22-inch aluminum shield was mounted to the socket to further direct the light skyward (figure 4).

Up to eight 1000w lights could be powered by two 5500W gas generators. A six foot by ten foot utility trailer was used to transport the portable lighting system and the generators. Six 250W high pressure sodium lights, eight 1000W high pressure sodium lights, and two 5500W generators could be carried inside the trailer.

The 1000W high pressure sodium lamps produce 140,000 lumens. An average 100 watt incandescent household lamp produces 1500 lumens. The 1000W lamps used in this study are equivalent to approximately 93 100W household incandescent lamps.

Field Site Selection

It was necessary to select field sites that were completely dark and were not near any sources of light pollution. Selected sites had no observation of light when viewed in the DMSP OLS imagery. This ensured that the portable lighting source was responsible for any light observed in the DMSP OLS data collected during field experiments. The local overpass time of the satellite means that in the summer the sun sets after the overpass. Because of this, the clearest images are collected in the fall, winter, and spring. Most of the field experiments were carried out in the winter, so field sites had to be accessible at all times of year by a truck and 6 foot by 10 foot utility trailer (figure 5).

The high pressure sodium lights give off a red/orange light that is viewable from a significant distance. Anecdotal evidence suggests the lights were visible to the human eye from up to 5 miles away across flat land. It is easy to mistake the glow from the portable light source for a wild fire due to the color. Given this it was also important to have permission from local land managers and law enforcement prior to carrying out the field experiments. Consequently site selection was further limited to sites where acquiring the appropriate permissions was possible.

Eventually three sites were chosen (figure 6) in Colorado and New Mexico. The sites were on the Pawnee National Grasslands in northeastern Colorado, the Karval State Wildlife Area in eastern Colorado, and the Santa Fe National Forest in northern New Mexico. Each site was easily accessible at all times of year, was far enough from neighboring light sources to be dark in the DMSP OLS data, and permissions from the land managers and local law enforcement were acquired.

Field Data Collection

Using available ephemeris data for the DMSP OLS it was possible to predict the overpass time of the satellite at the different field sites. The predictions proved to be within seconds of the actual overpass times. Field experiments were planned for nights when the lunar illuminance was less than 0.0005 lux and the solar elevation was less than -12 degrees. These requirements ensured there was no moon light or sun light contamination in the imagery during field collections. Weather was also considered and trips were planned for nights that were likely to have clear skies as clouds can obscure the light in the DMSP OLS imagery. Despite planning efforts the weather did not always turn

out as predicted. Imagery collected of the field experiments that was found to have cloud cover were excluded from the analysis process.

During each field experiment the portable lighting system was deployed at the site an hour prior to the predicted overpass time. High pressure sodium lights to not achieve their full brightness at ignition. In order to ensure full brightness the lights were turned on at least 45 minutes prior to the predicted overpass. Although the overpass predictions proved to be accurate within seconds of the actual overpass, the lights were left on for at least 15 minutes after the predicted overpass to ensure coverage. During the time of the field experiments from December 2009 – January 2011 there were two DMSP satellites flying with the OLS onboard (F16 & F18). Depending on the geometry of the satellite on any given night it was possible to have the field site viewed once or twice by each satellite. The portable light was always turned on 45 minutes or more before the initial predicted overpass and turned off no earlier than 15 minutes after the last predicted overpass. The entire lighting system was packed up and removed from the sites after every experiment.

DMSP OLS Data

DMSP OLS data for each field experiment were acquired from the National Geophysical Data Center (NGDC) in Boulder, CO (NOAA/NGDC, 2012). The imagery was processed and geolocated in accordance with the methods described in Baugh et al. (Baugh et al., 2010) and Elvidge et al. (Elvidge et al., 2001b).

The data acquired came in the form of GeoTiffs and included several images for each orbit. The included images were the visible band imagery, thermal band imagery, samples image, and gain image. The visible image contains digital number (DN) values

ranging from 0-63. The thermal image contains digital number ranging from 0-255. The samples image contains a value representing the sample in the image and allowed for the calculation of scan angle of each observation. The gain image contains values representing the gain for each pixel in the visible band image and allows for the conversion of the visible image DNs into radiance values.

The OLS data is collected at a resolution of 0.6km, referred to as fine data. A limited quantity of this data can be recorded between downloads. Additionally, the data is resampled to 2.7km, by averaging a 5x5 grid of fine pixels, onboard the satellite. The resampled data, referred to as smooth data, can be collected globally each day. The Air Force Weather Agency (AFWA) determines where the fine data will be collected at any given time. During this research a request was made to AFWA to collect fine data over the study area and it was granted. During the study, data was collected from both satellites F16 and F18 in both the smooth and fine resolutions.

Data Analysis

A total of 26 images were collected of the portable lighting source that met all the criteria described in section 2.3. Different quantities of light were used on different nights ranging from 1000W – 8000W. The ground footprint of the OLS is larger than the pixel size (Elvidge et al., 2004b) and the portable light source was always detected in multiple pixels. For each image a polygon was created that outlined the pixels in which the portable light source was detected.

Using the polygons outlining the light in the imagery the average DN, average gain, and average sample within the polygons were extracted from the visible, sample, and gain images. Using the average DN and average gain, the radiance observed for each

collection was calculated. The average sample was used to calculate the average scan angle for each observation of the portable light source. On each night of a field experiment the number of watts of lights used was recorded.

A table was constructed that contained the satellite identifier (F16 or F18), the average scan angle, the watts of light used, and the resolution of the data (fine or smooth). The average scan angle was used to calculate the distance from the portable light source to the sensor to account for optical depth. This distance was then used to calculate the inverse distance squared.

The table was then imported into JMP® Pro to analyze the data. Linear regression analyses were performed to evaluate the correlation between the brightness of the lights on the ground and the observed data values in the visible band imagery. Although watts are not a measure of brightness it was used here to represent the brightness of the lights used on a given night. Since all the lamps were of the same type (Sylvania Lumalux High Pressure Sodium) the watts were considered to be a valid proxy of the brightness of the lights. The observed radiance was the dependent variable and satellite (nominal), spatial resolution (nominal), brightness of the lights (represented by watts), and optical depth ($1/\text{distance to sensor}^2$) were the independent variables.

Varying amounts of light ranging from 750W to 8000W of high pressure sodium were used on different nights. It was observed that as little as 1000W of high pressure sodium could be observed by the OLS during these trials. In an effort to define the minimum detectable brightness of the OLS, four images were further examined from a night when 1000W of high pressure sodium were fielded and observed.

The images consisted of smooth and fine resolution images from each satellite. In each image, a collection of pixels representing noise was identified and the mean and standard deviation were calculated. The mean plus one standard deviation was defined as the noise boundary. Next, the maximum brightness of pixels identified as the portable light source was recorded. It is possible to identify very dim lights in the imagery through manual inspection and by correlating the location with high resolution imagery available in Google Earth. Each image was inspected to select lights with a lower DN than the portable light. The mean and standard deviation of the dim lights was calculated and the minimum detectable DN was defined as the mean. These lower values were used to estimate the signal to noise ratio and the minimum detectable brightness of the OLS.

Results and Discussion

During this study different quantities of lamps were used on different nights. The experiments ranged from one 1000W lamp up to eight 1000W lamps at a time. It was found that eight 1000W lamps produce enough energy to saturate the higher resolution fine data collected by the OLS. They did not, however, produce enough energy to saturate the lower resolution smooth data collected by the OLS. One 1000W lamp produced enough energy to be detected by the OLS in both the smooth and fine resolution data. This suggests that as few as ninety-three 100 watt incandescent lamps could be observed by the OLS.

The results observed using one 1000W lamp suggest that the OLS may be capable of detecting lights producing less energy. It would be valuable to conduct further studies with lamps under 1000Ws. This would allow a confirmation of the minimum detectable

brightness of the OLS. Further studies are needed to confirm whether or not one 1000W high pressure sodium lamp is the minimum detectable.

On 8 January 2011 1000W of high pressure sodium was fielded and observed by both satellites F16 and F18 in and recorded in both the smooth and fine resolution. Each of these four images was further investigated in an effort to determine if the minimum detectable brightness is below 1000W of high pressure sodium. The results of this investigation are reported in table 4. The minimum noise boundary, the DN of manually identified dim lights, and the maximum DN associated with the portable light observations are shown. The signal to noise ratio (S/N) for each image was calculated as: minimum DN / noise boundary DN. For the smooth data the S/N was approximately 2:1 and for the fine data was about 2.4:1. This process also allowed for estimates of the minimum detectable brightness below the known limit of 1000W of high pressure sodium. Using the DN observed from the portable light and the DN of dim light found in the imagery below the portable light values the minimum detection was calculated as: dim light DN / portable light DN * 1000W. This analysis suggests that for smooth data the minimum datable brightness for smooth data may be approximately 900W of high pressure sodium. For fine data the results show it may be between 550W and 650W of high pressure sodium. There are differences in the values across the two satellites, which may be explained by a combination of factors including:

1. The F16 images were collected at a gain of 49 while the F18 images were collected at a gain of 57.
2. Differences in the sensitivity of the OLS on each satellite

The images were collected at approximately the same scan angle so this was not considered to be a factor in the differences.

Table 4: Results of minimum detectable brightness analysis

Satellite & Resolution	Noise Boundary (DN)	Dim Light (DN)	Portable Light (DN)	S/N	Minimum Detectable Watts
F16/Smooth	2.6	4.6	5	4.6:2.6	920
F18/Smooth	3.5	7.1	8	7.1:3.5	888
F16/Fine	4.9	11.5	21	11.5:4.9	548
F18/Fine	7.3	18.6	29	18.6:7.3	641

Radiance observed by the DMSP OLS is correlated with satellite, resolution, brightness of the lights (represented by watts), and optical depth (1/distance to sensor^2). The results of the linear regression modeling are shown in table 5. When attempting to model both satellites F16 and F18 the model resulted in an R^2 of 0.61, the actual by predicted plot for the model is shown in figure 12. Modeling each satellite individually resulted in higher R^2 values, which implies there is a significant difference in current spectral response of the OLS on the two satellites. When modeling satellite F16 the R^2 was 0.72 and for F18 the R^2 was 0.72. The actual by predicted plot for the satellite F16 model is shown in figure 13 and for the satellite F18 model it is shown in figure 14.

Table 5: Results of the Linear Regression Analysis

Satellite	**Equation**	**Rsquare**
F16 & F18	Radiance = 1.4296e-7 + 1.38e-12* Watts + -0.172516 * 1/OD^2 + -1.138e-9 * Sat[F16] + -7.014e-8 * Resolution[Smooth]	0.61
F16	Radiance = 2.8161e-7 + 1.38e-12* Watts + -0.172516 * 1/OD2 + -7.83e-8 * Resolution[Smooth]	0.72
F18	Radiance = 6.2462e-8 + 1.573e-11 * Watts + -0.011343 * 1/OD2 + -6.008e-8 * Resolution[Smooth]	0.72

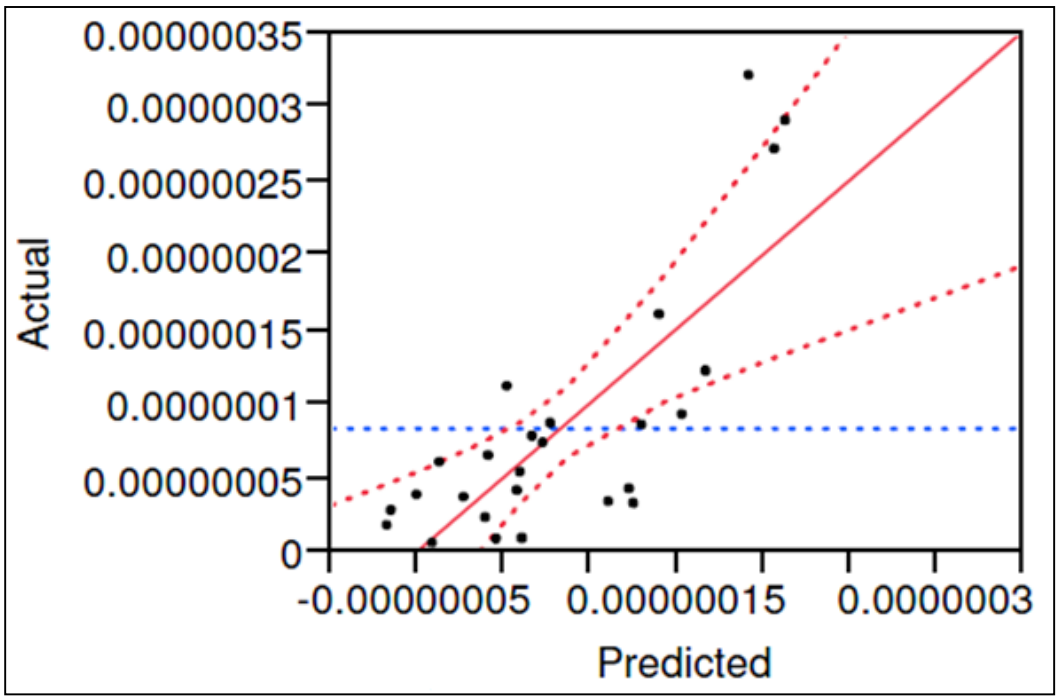

Figure 12: Actual by predicted plot for F16 & F18 regression model.

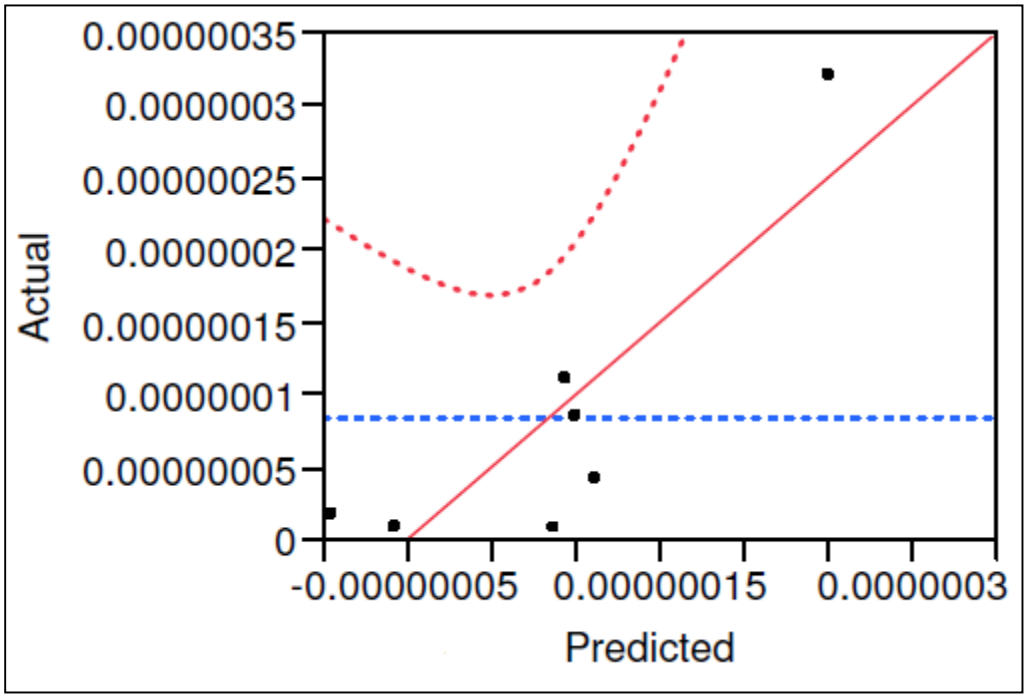

Figure 13: Actual by predicted plot for F16 regression model.

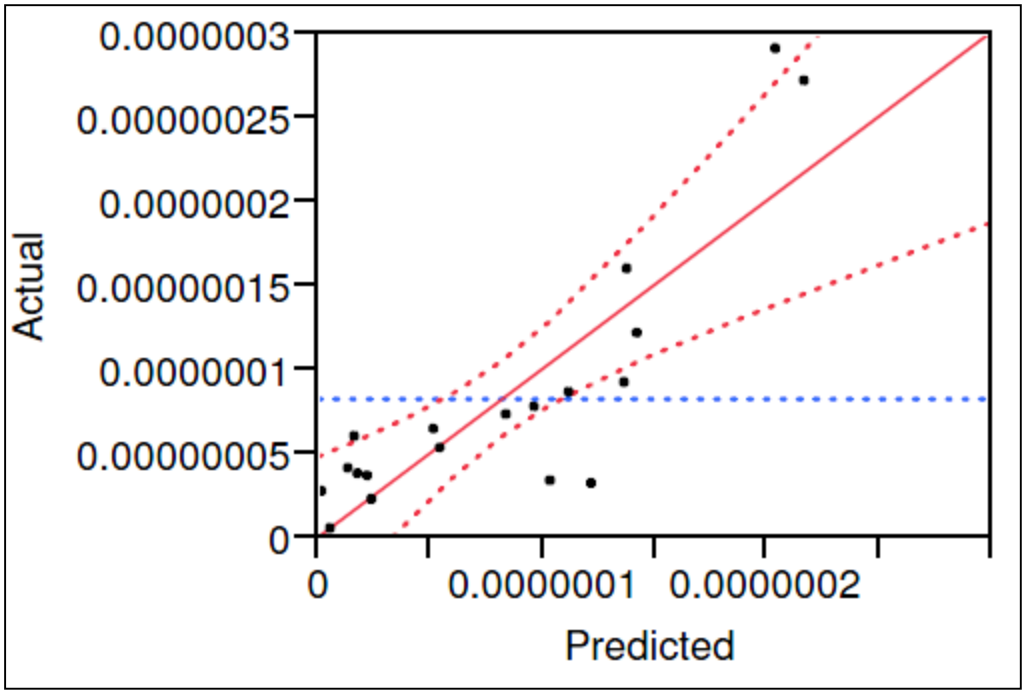

Figure 14: Actual by predicted plot for F18 regression model

The models show that satellite, resolution, brightness of the lights, and optical depth explain much of the variability in radiance observed by the OLS. It is expected that some portion of the unexplained variability is due to degradation of the sensor between December 2009 and January 2011. However, the degradation over that time may not account for all of the unexplained variation. Each night the thermal data from the OLS was examined to determine if the observation is cloud free. However, there is a chance that very light clouds could go undetected by the OLS and could have an impact on the observed DN. It is possible that using an atmospheric model in addition to optical depth would account for some of the unexplained variability. Another factor that may account for some of this unexplained variability is the oblong shape of the lamps used in these experiments. It is expected that the emitted energy of the lamps is not consistent from all angles. Taking the lamps to a lab to measure the Bidirectional Reflectance Distribution

Function (BRDF) and using the BRDF in conjunction with scan angle may also account for some of the unexplained variability. Lastly, the smooth data pixels are created by averaging a five pixel by five pixel grid of fine data. Depending on where the girds fall in the data the resulting radiance in the smooth data can be very different. For example, if the five by five grid was centered on the brightest fine pixels the resulting smooth pixel would have a high DN. However, if multiple five by five grids share the brightest fine pixels the resulting smooth pixels would have a lower DN. This process is certainly the cause of some of the unexplained variability.

Given the correlation between the brightness of the portable light source and the observed radiance this process should be valuable for radiance calibration. By deploying a light source of this type at a known location over long periods a record of the sensor response could be created. This record would allow for the creation of offsets to account for changes in spectral response of the OLS over time. Additionally, it would allow for offsets to account for differences in spectral response between two or more satellites with the OLS on board. These offsets would allow for more precise temporal and inter-satellite comparisons of OLS nighttime lights data. It would be valuable to have a location, with no surrounding lights, capable of supporting a long term installation of a light source of this nature.

In addition to the applicability of this process to the DMPS OLS, there are other applications. The recently launched VIIRS onboard NASA's Suomi National Polar-orbiting Operational Environmental Satellite System Preparatory Project (NPP) spacecraft would also benefit from the process defined here. VIIRS acquired its first measurements on 21 November 2011(NASA, 2012) and is capable of low light imaging

collection to produce nighttime lights imagery, similar to the DMSP OLS. Temporal and inter-satellite comparisons of VIIRS data would benefit from the portable light design and calibration process as well.

This process would also be applicable and beneficial to the proposed NightSat mission concept (Elvidge et al., 2007a; Elvidge et al., 2007c). The NightSat proposes a new sensor capable of global observations collected at a spatial resolution capable of delineating primary features of human settlements. This sensor also includes increased spectral resolution that would allow it to distinguish between different types of lamps, for example, distinguishing high pressure sodium from metal halide. To take advantage of this characteristic of NightSat, it would be valuable to include multiple lamp types in the process described here to increase the relevance.

Lastly, this methodology also has applications to nighttime photographs taken from the International Space Station (ISS) night (Anderson et al., 2010; Lulla, 2003). Astronauts onboard the ISS are able to take photos at night that present varying resolution color images of nighttime lights. These photographs are a valuable addition to satellite nighttime lights imagery for a wide array of research topics. Like the proposed NightSat these photos allow one to observe light sources with different spectral signatures. The process described here should be valuable for these ISS photos as well.

Conclusions

A portable light source capable of detection by the DMSP OLS was designed and fielded on 27 nights between December 2009 and January 2011. The light was deployed in locations with no surrounding light sources on nights with a lunar illuminance less than 0.0005 lux and a solar elevation angle less than -12 degrees. On 13 of those nights cloud

free imagery was collected with observations of the portable light source. The portable light was used in multiple lamp configurations ranging from one 1000W lamp to eight 1000W lamps. It was established that eight 1000W high pressure sodium lamps produce enough energy to saturate the fine resolution data, but not the smooth resolution data. Furthermore, it was determined that the DMSP OLS can detect as little as one 1000W high pressure sodium lamp.

DMSP OLS data was collected and acquired for the nights of the field experiments. The DN values were converted to radiance using the pre-flight spectral response of the OLS and the sensor gain at the time of collection. Linear regression was used to model radiance with the following parameters: satellite (nominal), spatial resolution (nominal), brightness of the lights (represented by watts), and optical depth ($1/\text{distance to sensor}^2$). A strong correlation between these variables and radiance was discovered.

This methodology can be used to improve temporal and inter-satellite comparisons if deployed at regular intervals. During this research it was necessary to remove the light source after each experiment. It would be valuable to find a dark location where the light could be deployed in a permanent or semi-permanent configuration. Such a deployment would allow the light could be turned on at the appropriate time nightly using a timer. Although weather would still preclude nightly observations this would provide a frequently observed light source at a known location and brightness for calibration. Moreover, this process should have relevance for both the VIIRS sensor and the proposed NightSat sensor and may improve the utility of nighttime photographs taken from the International Space Station. The current results and future

potential indicate that leaving a similar lighting system deployed in a fixed location long term would be of significant value for nighttime lights research and applications.

Future research in several areas is indicated. Field experiments should be conducted with lamps producing less energy than one 1000W high pressure sodium lamp. This would allow the minimum detectable brightness to be soundly defined. In addition, a detailed atmospheric model for each night of observation might improve the models. Lastly, a campaign carried out at regular intervals with the same number of lamps on each night would be valuable. The results suggest that such a campaign would allow for offsets accounting for sensor degradation and differences between the sensitivity of the OLS on different satellites to be accounted for. This would allow for improvements in the results of studies using temporal and inter-satellite data comparisons.

Chapter Four: Illuminating the Sky: Estimating the Global Energy Expended to Light the Night Sky

Introduction

Flying in to Denver International Airport at night one can look out the window and observe the city lit up below. The wide array of lighting that cities around the world put into place are visible at night, not just from the ground they are intended to light, but also from above. The Defense Meteorological Satellite Program (DMSP) Operational Linescan System (OLS) measures the light emissions around the globe nightly. The imagery of lights at night collected by the DMSP OLS are recognized for their value in a wide range of studies, including economic distribution (Doll et al., 2000; Ghosh et al., 2010b; Ghosh et al., 2010c), mapping urban extent (Elvidge et al., 2004c; Elvidge et al., 2007d; Henderson et al., 2003; Imhoff et al., 1997a; Imhoff et al., 1997b; Potere & Schneider, 2007; Schneider et al., 2003; Small et al., 2005), impacts of artificial lighting on various species (Kloog et al., 2008; Longcore & Rich, 2004), and mapping CO_2 emissions (Doll et al., 2000; Ghosh et al., 2010a). Additionally, these observations provide an opportunity to examine the energy wasted into the sky at night.

Groups such as the International Dark Sky Association and local governments concerned with light pollution have rallied to limit light pollution. Additionally, scientists have also become aware of the impact of artificial nocturnal lighting on species such as sea turtles, which can be distracted after hatching and wander away from the ocean

towards cities and their deaths. These realizations have resulted in a number of lighting ordinances (International-Dark-Sky-Association, 2012) around the USA minimizing artificial lighting or requiring shielding of lights. Recent events such as Earth Hour have encouraged cities and residents to turn out their lights to bring awareness to climate change and educate people on simple steps, such as turning off a light, which can be taken to alleviate the problem. In this paper a method for estimating the total energy used to light the night sky is presented. This process provides a repeatable mechanism to quantify the energy use associated with leaving lights on and not implementing light shielding regulations. This study allows us to begin quantifying the amount of energy that might be saved by improved regulations and light shielding.

Methods

Overview

DMSP OLS imagery was collected of a portable light source in locations with no existing light sources present. The amount of light used on each night of imagery collection was recorded. A DMSP OLS annual composite converted to radiance was acquired from NGDC. The radiance values in the composite were converted to watts of energy based on the model developed in Chapter 3. This allowed for global estimates of the energy expended each night on lighting the night sky. These numbers were normalized by Gross Domestic Product (GDP) and population. Data on the costs of energy in different countries were used to create estimates of the costs associated with the expended energy estimates.

Design and Configuration of the Portable Lights

The basis for this study was a portable lighting system capable of being observed by the DMSP OLS. A number of different lighting configurations were examined during the design phase and are described chapter 2. After a series of experiments it was determined that commercially available high pressure sodium lights, commonly used to light warehouses, were the best suited option for this study. This decision was based on a combination of factors including: 1) The watts to lumens ratio (high pressure sodium produces a higher number of lumens per watt than most other commonly available light sources); 2) High pressure sodium has a spectral peak in the orange between 600nm and 800nm (figure 2) that correlates with the peak spectral sensitivity of the OLS (figure 3) and is less prone to Rayleigh scattering than other lamp types.

High pressure sodium lamps require a ballast, capacitor, and igniter to start the lamp and to regulate the current once the lamp is ignited. All the necessary parts were framed so that the lamp was pointed straight up towards the sky and seated in a 22 inch aluminum reflector (figure 4). For these experiments eight portable lights were constructed, consisting of a 1000W high pressure sodium lamp. Each lamp emits 140,000 lumens, while the average 100 watt household incandescent lamp emits 1500 lumens. It would take approximately 93 100W incandescent lamps to emit the same number of lumens as one 1000W high pressure sodium lamp.

Two 6000 watt gas generators were used to power all eight of the lights in remote locations and were capable of powering eight 1000W high pressure sodium lamps for upwards of 6 hours. This configuration (including the lights and generators) was capable

of being transported in a 6 foot by 10 foot utility trailer (figure 5). The entire system could be easily transported from one site to another and deployed in 30 minutes.

Field Experiments

To carry out the field experiments it was necessary to find sites that were completely devoid of light. This ensured that any light observed by the OLS in these areas was emitted by the portable light. Sites were selected first by examining annual composites of DMSP OLS imagery (Baugh et al., 2010; Elvidge et al., 2001b; Ziskin et al., 2010) as well as nightly imagery to determine if there was any detectable light in the area. Sites deemed suitable from imagery were visited to confirm that no lights were present in the area. All the sites selected were on public lands and the orange glow emitted by the lights was easily confused with fire from a distance at night. Thus the final step in site selection was to obtain permission from both local land managers and local law enforcement agencies.

A total of three suitable sites were selected based on the site selection criteria (figure 6). The final sites were: the Pawnee National Grasslands in northeastern Colorado; the Karval State Wildlife Area in eastern Colorado; and the Santa Fe National Forest in northern New Mexico. Summer time observations of the DMSP OLS in these locations are negatively impacted by solar glare. Consequently, all of the field experiments were carried out in the winter. Each site was accessible through the winter by a truck towing the utility trailer.

We chose the dates for these field experiments using a combination of weather forecasts, lunar phase calculations, and solar elevations at the time of the DMSP OLS

overpass. Although the weather did not always turn out as predicted, the goal was cloud free nights for each experiment. After carrying out a field experiment the data were rejected if it turned out to be cloudy. Additionally, only nights with a lunar illuminance less than 0.0005 lux and a solar elevation less than -12 degrees were deemed valuable; this ensured no contamination from moonlight or sunlight in the imagery.

On nights that met the criteria for the experiments the lights were driven to one of the three sites. The overpass time was predicted in advance and proved to be accurate to within seconds of the actual overpass time. Since high pressure sodium lamps take some time to warm up to their full brightness the lamps were always turned on at least 45 minutes prior to the predicted observation time. On each night the entire lighting system was packed up and removed from the site, no materials were ever left over night.

DMSP OLS Annual Radiance Composite

The National Geophysical Data Center (NGDC) in Boulder, CO produces annual composites from the DMSP OLS data. An annual composite that had been converted to radiance values (Ziskin et al., 2010) was acquired from NGDC. This product was created using data from satellite F16 for the year 2010. DMSP OLS data are collected at two resolutions; 1) 0.6km^2 known as fine; 2) 2.7km^2 known as smooth. The smooth data is collected globally each night while the fine data is only collected for certain portions of the globe on each night. The annual composites are made with smooth data.

The annual composite contained pixel values representing the average nightly radiance from 180° West to 180° East and 65° South to 75° North. This product is made from cloud free imagery and uses only the center 60% of the orbital swath to minimize

any effects of distortions present at the edges of the imagery. This data is also processed using the same thresholds for lunar illuminace (less than 0.0005 lux) and solar elevation (less than 12 degrees) as used in this study.

The annual composite contained lights representing cities, towns, and villages as well as gas flares (Elvidge et al., 2007b; Elvidge et al., 2001b; Elvidge et al., 2009c). NGDC has produced a series of vectors outlining the location of gas flares around the globe. Using these vectors a mask was created to filter the gas flares out of the annual composite. This was done to avoid overestimating the watts expended by including gas flares in the calculations.

Landscan Population

Landscan population data was acquired from the Oak Ridge National Laboratory. The Landscan population dataset represents ambient population around the world (Bhaduri et al., 2002). The data are gridded at a resolution of 30 arc-seconds by 30 arc-seconds globally. Landscan ambient population estimates for the year 2008 were used for this research.

Gross Domestic Product Estimates

Official statistics on GDP have a number of shortcomings in the collection process and often exclude the informal economy (Ghosh et al., 2010b). To address these shortcomings Ghosh et al. (2010b) used the sum of lights from annual composites of DMSP OLS imagery to predict GDP globally. This was done by building regression models calibrating the sum of lights to sub-national measures of economic activity for

China, India, Mexico, and the United States. These estimates are made available by the NGDC as a 30 arc-seconds by 30 arc-seconds grid of the world.

International Electricity Prices and Fuel Costs

The US Energy Information Administration (EIA) publishes annual data on international electricity prices and fuels costs (US-Energy-Information-Administration, 2008). The prices are published by country per year. The most recent available prices were from the year 2008.

Data Analysis

Development of Regression Equations

Between December 2009 and January 2011 the light was deployed to the field and a total of 28 images were collected that met the criteria described in section 2.1 for two satellites (F16 & F18) and at two resolutions (smooth & fine). Six of those images were collected during the year 2010 by satellite F16 in the smooth resolution. Linear regression was used to establish a correlation between the radiance and the watts of light used on each night. Observed radiance was set as the dependent variable and satellite (nominal), spatial resolution (nominal), brightness of the lights (represented by watts), and optical depth (1/distance to sensor^2) were set as the independent variables.

Application of Regression Equations

The equations determined by linear regression were applied to the annual composite to convert from radiance to watts. Next the sum of watts was extracted from the imagery at two administrative levels. One extraction was done using country borders to determine the sum of watts by country. A second extraction was performed using state

borders to determine the sum of watts by state around the world. These extractions allowed for tables and maps to be created showing the sum of watts at the country and state level administrative levels.

Results and Discussion

The result of the linear regression model show that radiance observed by the DMSP OLS correlates with resolution, brightness of the lights (represented by watts), and optical depth (1/distance to sensor^2). An R^2 of 0.72 was reported for equation 3 which is specific to satellite F16. Equation 3 was used to convert the annual composite from radiance to watts with minor alterations.

Radiance = 2.8161e-7 + 1.38e-12 * Watts + -0.172516 * 1/OD2 + -7.83e-8 * Resolution[Smooth]

Equation 3: Regression model to predict radiance for satellite F16.

For the annual composite average scan angle is not recorded. Scan angle was used to determine the optical depth. It is expected that since only the center 60% of the orbital swath is used to generate composites and it is an average of many observations that dropping this factor averages out. Additionally, only smooth resolution data was used so the resolution component of the equation was also dismissed. The radiance was converted to watts using equation 4.

Watts = (Radiance / 1.38e-12) - 2.8161e-7

Equation 4: Equation used to convert radiance to watts.

Using the equations described above an image was created in which the value of each cell is the estimated Wh expended as observed by the sensor (figure 15). As the sensor only observes a brief moment in time the energy value is represented as Wh.

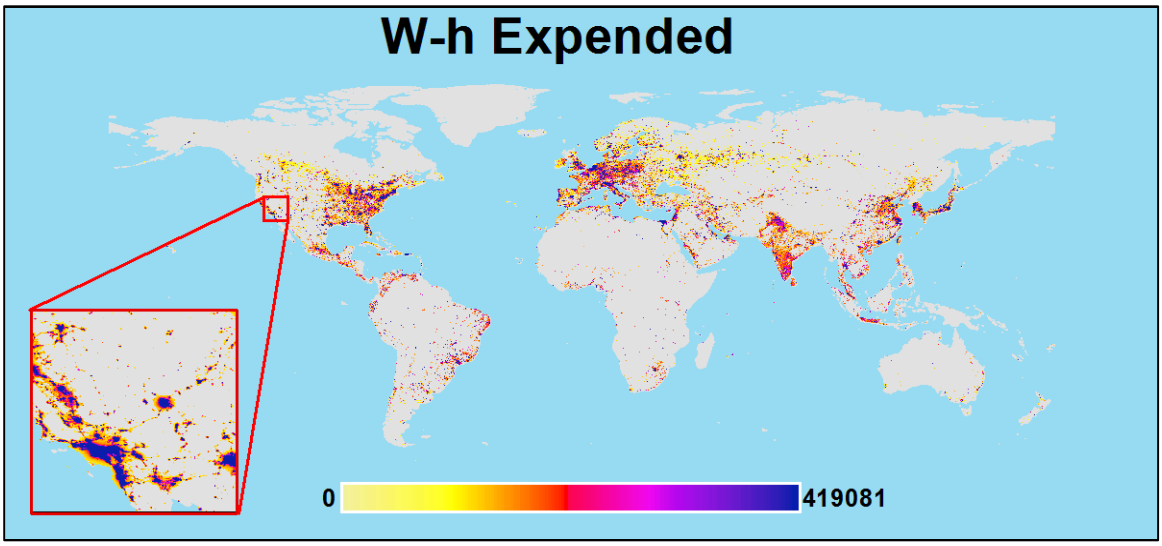

Figure 15: Map of Wh expended during a satellite overpass.

The Wh expenditures grid was used as the basis for calculating the statistics by country and by state. Figure 16 shows a graph of the top 20 countries with the expenditures per night expressed as MWh. The United States is in first and expends more than double the second (China) and third (Russia) place holders and India in the fourth place position is only slightly behind Russia. After India there is another significant drop in expenditures, stepping down to Brazil in the fifth position and Canada in the sixth position. From there a steady decrease is seen moving from Japan in the seventh position out to Sweden at number 20. Figure 17 shows a map of the expenditures in MWh for each country across the globe. Figure 18 displays a graph of the top 20 states

expenditures in kWh. Texas, in the USA, holds the first position and there is a steadier decline, than seen in the countries graph, moving from place one to 20, Shandong, China. Figure 19 is a map of the kWh expended per state across the globe and highlights the states in each country with the highest expenditures per night. Table 6 contains the estimated expenditures for every country in MWh.

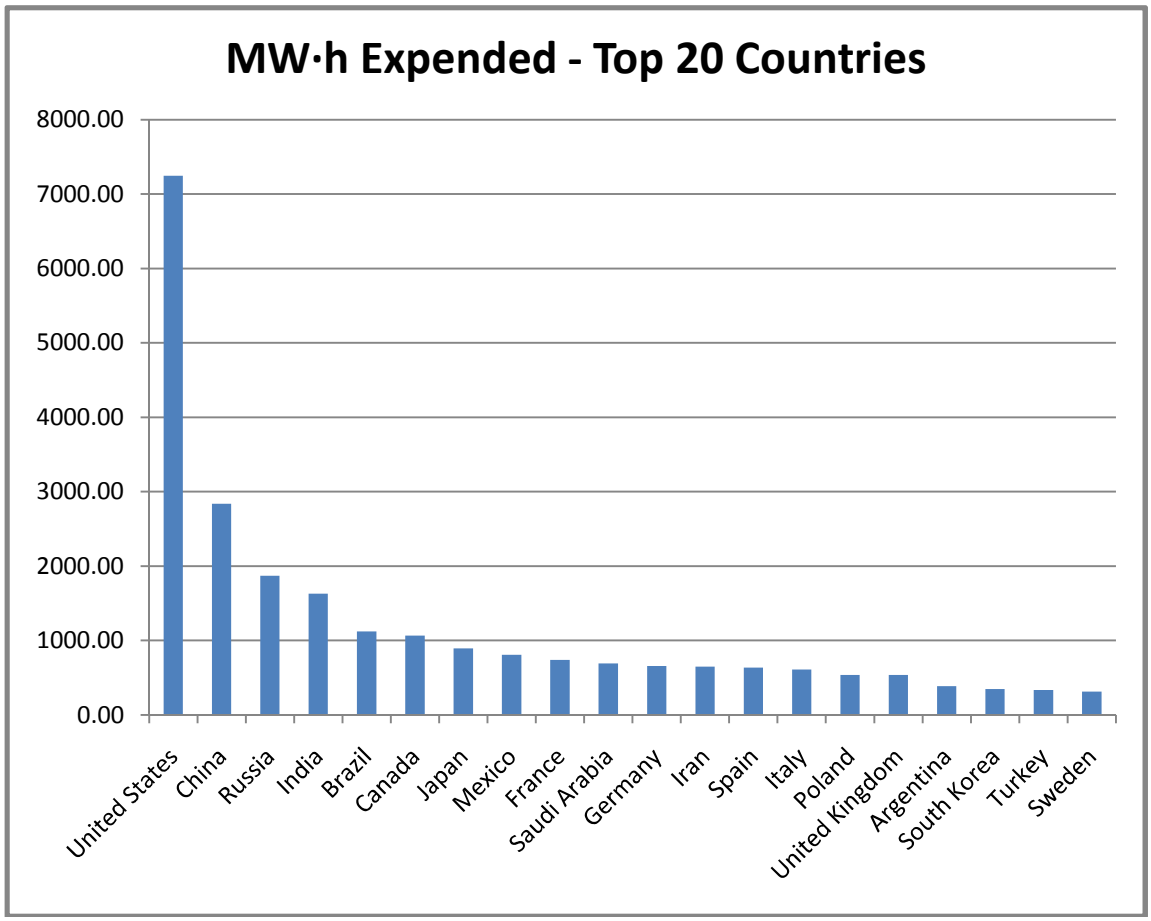

Figure 16. Graph of the top 20 countries megawatts per night.

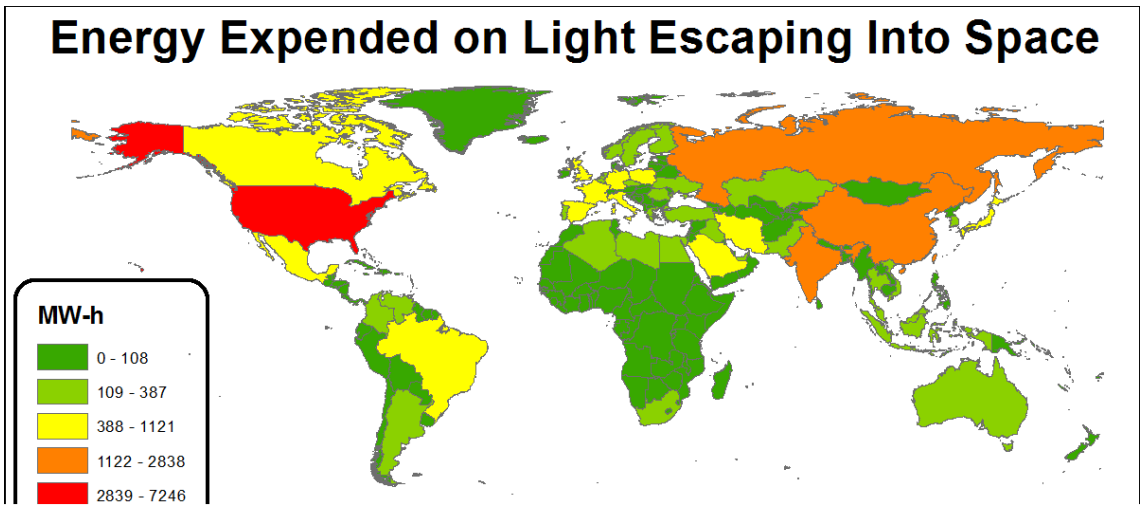

Figure 17: Map of MWh expended per country.

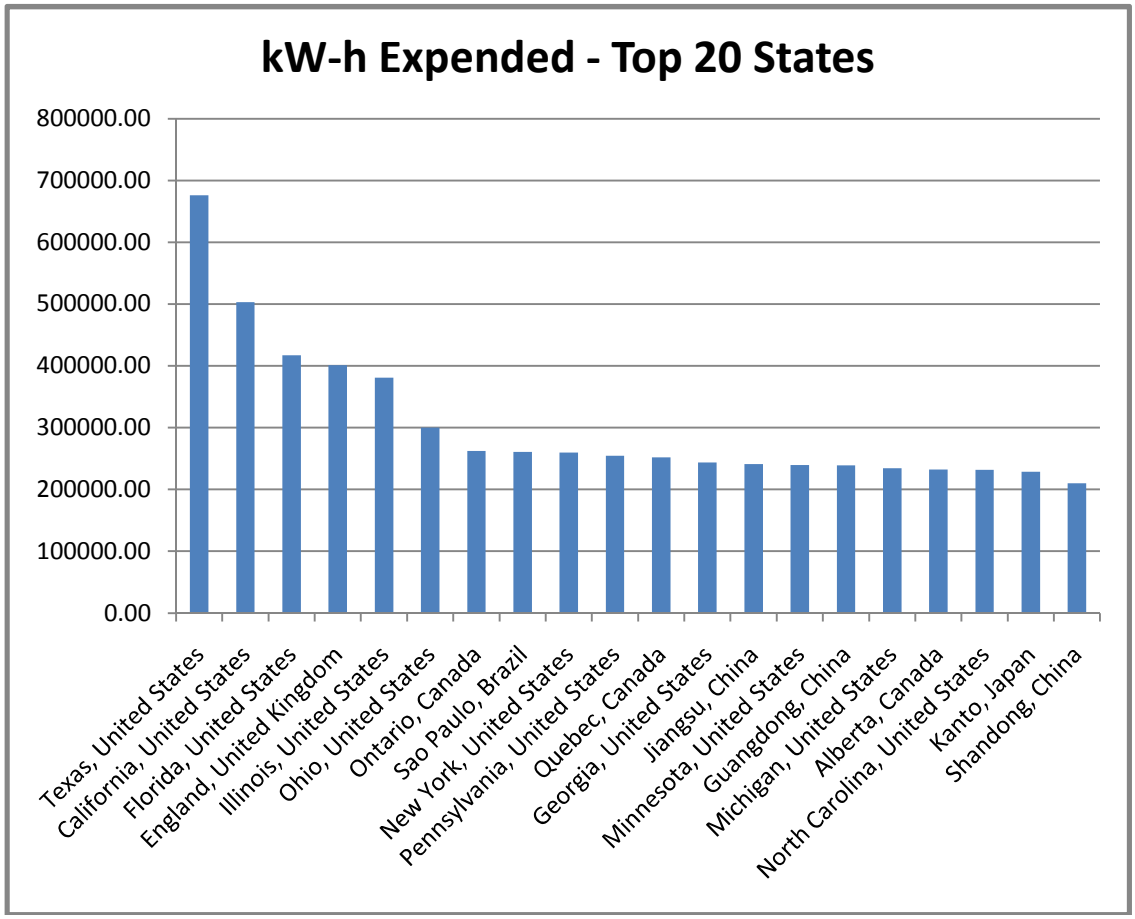

Figure 18: Graph of the top 20 states kilowatts expended per night.

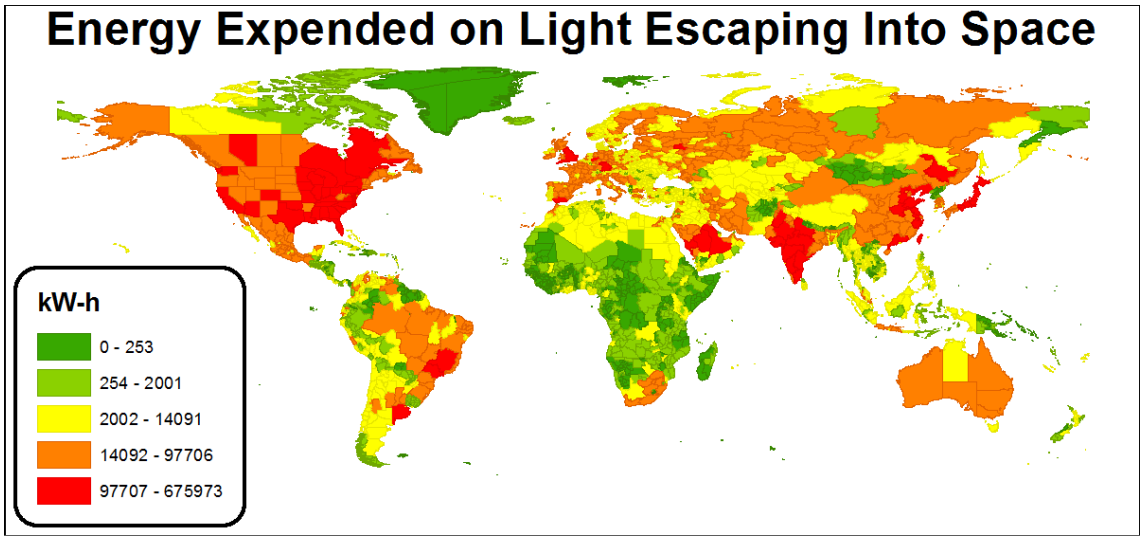

Figure 19: Map of states kWh expended by state.

Table 6: Megawatts expended per night by country.

Country	MWh	Wh/GDP	Wh/Pop
Afghanistan	12.47	433.01	0.38
Albania	9.01	398.77	2.59
Algeria	162.58	620.84	4.90
American Samoa	0.21	1061.21	3.72
Andorra	1.18	259.73	14.27
Angola	24.80	302.91	2.00
Anguilla	0.18	5352.28	14.09
Antigua & Barbuda	0.85	573.01	10.55
Argentina	386.60	646.57	9.54
Armenia	8.68	474.15	2.92
Aruba	0.83	324.99	9.39
Australia	211.02	241.35	10.35
Austria	92.41	257.01	11.32
Azerbaijan	29.89	453.24	3.67
Bahrain	19.19	731.34	32.78
Bangladesh	39.53	186.72	0.26
Barbados	1.63	312.45	6.94
Belarus	107.60	906.49	11.12

Country	MWh	Wh/GDP	Wh/Pop
Belgium	119.65	276.49	11.45
Belize	3.12	1062.65	10.57
Benin	4.09	304.53	0.48
Bermuda	0.08	166.52	7.19
Bhutan	1.10	350.11	1.40
Bolivia	33.52	708.87	3.64
Bosnia & Herzegovina	21.00	645.47	4.61
Botswana	7.46	264.09	4.04
Bouvet I.	0.00	0.00	0.00
Brazil	1120.73	532.23	5.82
British Indian Ocean Territory	0.06	0.00	0.00
British Virgin Is.	0.19	752.43	8.92
Brunei	6.35	305.06	19.36
Bulgaria	54.57	556.57	7.55
Burkina Faso	4.59	235.84	0.30
Burundi	0.67	233.80	0.08
Cambodia	7.07	276.53	0.50
Cameroon	6.45	147.13	0.35
Canada	1065.21	701.57	30.76
Cape Verde	1.31	781.87	3.46
Cayman Is.	0.56	329.68	19.88
Central African Republic	0.46	167.07	0.10
Chad	1.96	112.35	0.19
Chile	95.78	370.84	6.11
China	2838.13	316.11	2.10
Christmas I.	0.04	0.00	28.06
Cocos Is.	0.00	0.00	114.65
Colombia	165.37	455.70	3.71
Comoros	0.30	836.14	0.48
Congo	3.49	221.79	0.88
Congo, DRC	10.15	481.54	0.15
Cook Is.	0.05	3727.36	6.86
Costa Rica	29.12	553.52	6.94
Cote d'Ivory	26.41	701.43	1.36
Croatia	56.39	721.98	13.58
Cuba	37.54	298.06	3.33
Cyprus	16.36	655.95	21.28
Czech Republic	141.86	496.25	13.83

Country	MWh	Wh/GDP	Wh/Pop
Denmark	64.44	288.76	12.44
Djibouti	0.56	602.27	2.29
Dominica	0.33	1005.48	7.70
Dominican Republic	24.40	352.97	2.59
Ecuador	65.99	574.58	4.86
Egypt	310.61	666.28	3.84
El Salvador	16.02	334.16	2.29
Equatorial Guinea	0.86	254.82	1.72
Eritrea	1.15	295.95	0.21
Estonia	34.24	1077.51	27.10
Ethiopia	9.56	164.07	0.12
Falkland Is.	0.17	9189.43	59.83
Faroe Is.	1.26	3187.92	33.81
Fiji	2.32	536.51	2.92
Finland	249.28	1132.13	47.77
France	737.14	308.55	12.12
French Guiana	1.73	74995.88	12.23
French Polynesia	1.16	271.98	6.05
French Southern & Antarctic Lands	0.15	0.00	0.00
Gabon	3.31	177.54	2.56
Gaza Strip	1.10	518.17	0.82
Georgia	12.55	576.23	2.79
Germany	657.59	206.78	8.00
Ghana	23.68	655.10	1.02
Gibraltar	0.07	2733.37	219.83
Greece	112.04	272.76	11.11
Greenland	0.18	556.75	0.42
Grenada	0.41	603.13	5.49
Guadeloupe	3.45	0.00	8.95
Guam	1.96	656.79	12.03
Guatemala	33.31	401.58	2.57
Guernsey	0.19	184.68	3.07
Guinea	1.55	132.98	0.17
Guinea-Bissau	0.14	218.23	0.09
Guyana	1.83	576.96	2.55
Haiti	2.43	201.41	0.30
Heard I. & McDonald Is.	0.03	0.00	0.00
Honduras	22.11	711.99	2.96

Country	MWh	Wh/GDP	Wh/Pop
Hungary	73.29	324.07	7.38
Iceland	9.06	690.25	17.91
India	1630.79	665.97	1.43
Indonesia	223.86	245.80	0.98
Iran	649.59	729.46	9.94
Iraq	113.03	914.73	4.30
Ireland	71.03	340.01	17.55
Isle of Man	0.61	191.90	8.70
Israel	80.55	402.33	12.05
Italy	609.16	292.23	10.78
Jamaica	11.68	472.43	4.33
Japan	891.98	189.53	7.31
Jersey	0.29	100.89	4.35
Jordan	40.98	1209.52	5.89
Kazakhstan	134.69	708.89	8.78
Kenya	11.60	181.83	0.31
Kiribati	0.02	8340.56	5.25
Kuwait	53.61	415.82	23.91
Kyrgyzstan	17.67	1446.89	3.37
Laos	6.34	467.67	0.95
Latvia	27.15	639.21	12.49
Lebanon	19.70	418.52	5.62
Lesotho	1.68	465.54	0.80
Liberia	0.89	656.20	0.29
Libya	114.22	1252.98	18.66
Liechtenstein	0.41	136.26	11.36
Lithuania	40.87	622.20	11.46
Luxembourg	7.11	168.94	14.39
Macedonia	10.57	514.30	5.10
Madagascar	2.24	118.21	0.11
Malawi	4.06	345.61	0.29
Malaysia	171.24	435.02	7.21
Maldives	0.02	0.00	0.31
Mali	5.20	335.07	0.42
Malta	3.29	332.14	8.85
Marshall Is.	0.01	6868.60	21.89
Martinique	4.05	0.00	10.25
Mauritania	2.43	348.16	0.72

Country	MWh	Wh/GDP	Wh/Pop
Mauritius	3.57	225.43	2.86
Mayotte	0.43	927.13	2.61
Mexico	806.66	565.45	7.40
Micronesia	0.16	1080.02	4.51
Moldova	12.92	1088.86	3.09
Monaco	0.16	333.75	4.14
Mongolia	7.46	789.27	2.50
Montserrat	0.04	15018.11	14.27
Morocco	86.51	590.76	2.60
Mozambique	9.92	526.20	0.47
Myanmar	36.96	766.07	0.79
Namibia	7.08	564.12	3.48
Nauru	0.02	18407.00	3.17
Nepal	6.94	207.84	0.23
Netherlands	126.24	178.31	7.68
Netherlands Antilles	1.78	611.07	10.01
New Caledonia	2.08	548.55	10.40
New Zealand	33.28	271.49	8.55
Nicaragua	10.82	561.43	1.88
Niger	3.27	309.49	0.25
Nigeria	74.34	265.69	0.51
Niue	0.01	4993.33	10.90
Norfolk I.	0.02	0.00	10.13
North Korea	3.86	98.88	0.17
Northern Mariana Is.	0.33	477.70	4.48
Norway	185.91	690.12	44.51
Oman	78.37	1218.58	24.83
Pakistan	275.52	562.94	1.60
Palau	0.08	2238.30	5.96
Panama	14.53	391.14	4.48
Papua New Guinea	3.63	270.94	0.66
Paraguay	29.42	918.52	4.31
Peru	76.60	325.52	2.65
Philippines	71.63	236.44	0.81
Poland	537.26	750.07	14.01
Portugal	141.46	517.71	13.64
Puerto Rico	38.26	421.88	9.89
Qatar	67.46	968.60	84.25

Country	MWh	Wh/GDP	Wh/Pop
Reunion	4.83	0.00	7.75
Romania	122.95	441.65	5.52
Russia	1867.76	785.79	12.88
Rwanda	1.08	146.53	0.11
Samoa	0.37	1239.29	2.18
San Marino	0.28	283.55	10.15
Sao Tome & Principe	0.22	2525.18	1.19
Saudi Arabia	690.60	1018.97	25.06
Senegal	7.24	314.82	0.57
Serbia & Montenegro	75.27	732.96	7.66
Seychelles	0.30	670.37	4.68
Sierra Leone	0.45	149.24	0.07
Singapore	18.74	90.98	4.33
Slovakia	42.77	362.56	7.82
Slovenia	23.67	387.85	11.93
Solomon Is.	0.13	402.89	0.42
Somalia	1.00	166.99	0.11
South Africa	237.25	438.79	4.88
South Georgia & the South Sandwich Is.	0.04	0.00	0.00
South Korea	345.46	265.25	7.47
Spain	637.36	406.85	16.12
Sri Lanka	37.72	413.87	1.84
St. Helena	0.03	0.00	4.94
St. Kitts & Nevis	0.28	876.65	9.93
St. Lucia	0.85	444.47	5.73
St. Pierre & Miquelon	0.08	0.00	11.70
St. Vincent & the Grenadines	0.27	678.51	3.27
Sudan	38.50	430.50	0.96
Suriname	4.35	993.56	9.19
Swaziland	3.12	466.94	2.78
Sweden	313.35	831.00	36.21
Switzerland	67.60	201.82	8.78
Syria	93.69	850.21	4.58
Tajikistan	9.57	685.91	1.33
Tanzania	9.54	207.23	0.24
Thailand	288.13	489.56	4.44
The Bahamas	3.76	463.39	13.95
The Gambia	0.88	478.58	0.51

Country	MWh	Wh/GDP	Wh/Pop
Timor Leste	0.37	382.64	0.34
Togo	2.21	370.37	0.38
Tonga	0.20	1113.09	3.46
Trinidad & Tobago	20.10	767.71	21.98
Tunisia	60.92	699.28	6.05
Turkey	332.48	448.45	4.77
Turkmenistan	47.59	1730.70	9.11
Turks & Caicos Is.	0.09	4314.51	21.17
Tuvalu	0.00	0.00	4.84
Uganda	4.39	141.80	0.14
Ukraine	253.92	694.00	5.54
United Arab Emirates	168.18	1002.44	40.44
United Kingdom	536.26	225.59	9.00
United States	7246.01	448.84	24.27
Uruguay	22.28	534.46	6.43
Uzbekistan	82.38	1066.05	3.00
Vanuatu	0.77	2142.79	5.21
Vatican City	0.04	246.91	4.19
Venezuela	218.37	586.41	8.52
Vietnam	128.18	530.35	1.52
Virgin Is.	1.39	782.22	14.36
Wake I.	0.01	0.00	0.00
Wallis & Futuna	0.04	28687.68	7.04
West Bank	16.73	875.20	6.51
Western Sahara	2.13	1754.00	5.81
Yemen	44.44	733.02	1.97
Zambia	12.54	667.32	1.06
Zimbabwe	8.05	2414.02	0.71

The 30 arc-seconds by 30 arc-seconds grid of GDP estimates was used to tabulate the GDP of every country and state around the globe. The Wh estimates collected for each country and state were divided by the GDP estimates. Using these numbers maps were made at the country and state level showing the estimated Wh divided by the estimated GDP. Figure 20 shows the Wh normalized by GDP for each country. The

highest ranked countries when normalized by GDP are small countries such as French Guiana, Wallis and Futuna, Nauru, and Montserrat. However, countries such as Zimbabwe, Turkmenistan, Kyrgyzstan, Libya, Finland, and Belize are also among the higher ranking countries. Table 6 also included the Wh divided by GDP data for each country. Figure 21 shows a map of Wh divided by GDP for each state. The highest ranked states are rather small and are difficult to pick out on the map. The highest rank states (represented on the map in red) are Saint-Laurent-du-Maroni, French Guiana; Cayenne, French Guiana; Wallis & Futuna; Nauru; Montserrat; Marshall Islands; Falkland Islands; Kiribati; Mondol Kiri, Cambodia; Guantanamo Bay, United States; San Andres y Providencia, Colombia; Al Khawr, Qatar; At Ta'min, Iraq; Anguilla.

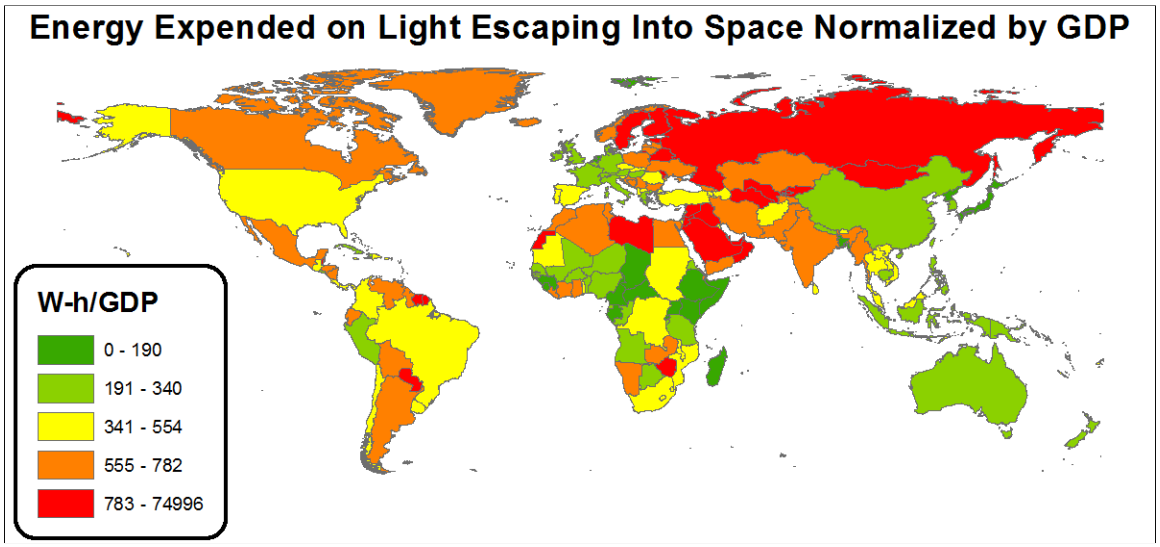

Figure 20: Map of states Wh/GDP expended by country.

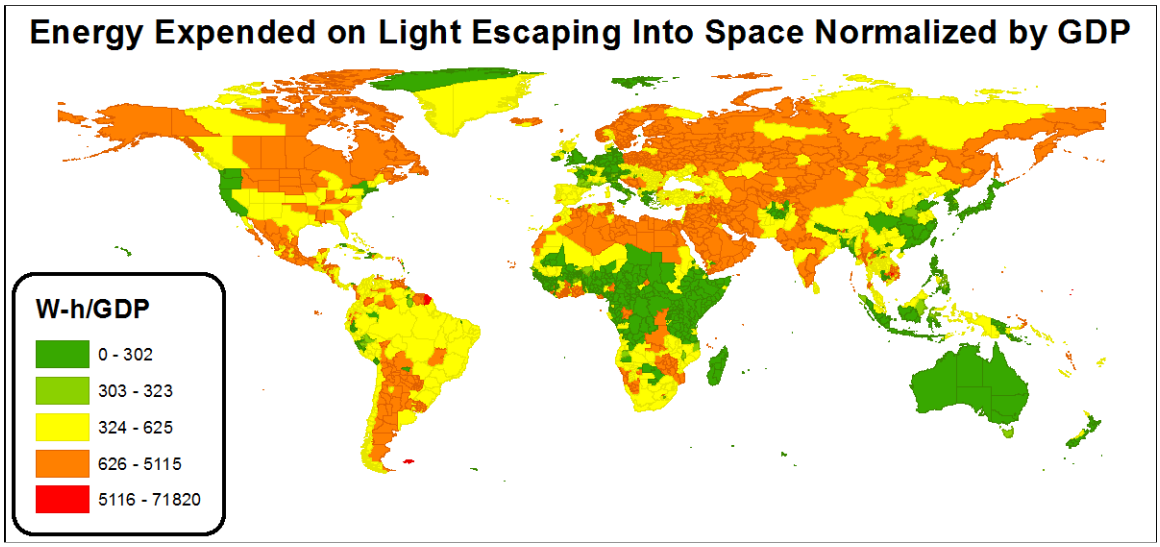

Figure 21: Map of states Wh/GDP expended by state, states in the red category are difficult to discern and consist of: Saint-Laurent-du-Maroni, French Guiana; Cayenne, French Guiana; Wallis & Futuna; Nauru; Montserrat; Marshall Islands; Falkland Islands; Kiribati; Mondol Kiri, Cambodia; Guantanamo Bay, United States; San Andres y Providencia, Colombia; Al Khawr, Qatar; At Ta'min, Iraq; Anguilla.

The Landscan population estimates were used to tabulate the ambient-population of every country and state around the globe. The Wh estimates collected for each country and state were divided by the population estimates. Using these numbers maps were made at the country and state level showing the estimated Wh divided by the estimated population. Figure 22 shows the Wh normalized by Landscan population for each country. Similarly to the GDP normalized numbers the highest ranked countries when normalized by population include small countries such as the Cocos Islands, the Falkland Islands, the Marshall Islands, as well as Trinidad & Tobago. Much larger countries are also in the highest ranking list including Finland, Norway, the United Arab Emirates, Sweden, Canada, Saudi Arabia, and the United States. Table 6 also included the Wh divided by population data for each country. Figure 23 shows a map of Wh divided by

population for each state. The highest ranked states are, like the Wh/GDP per state data, rather small and are difficult to pick out on the map. The highest rank states (represented on the map in red) are San Andres y Providencia, Colombia; Jarayan al Batnah, Qatar; Al Khawr, Qatar; Guantanamo Bay, United States; Ash Shamal, Qatar; Madinat Hamad, Bahrain; Al Jumayliyah, Qatar; Al Jawf, Yemen; Al Ghuwayriyah, Qatar.

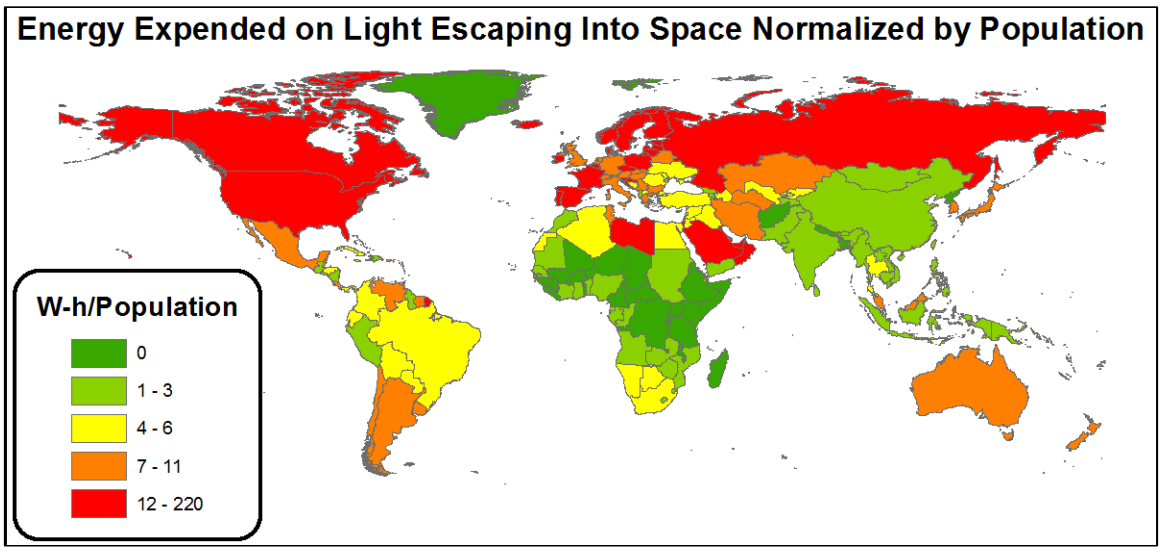

Figure 22: Map of states Wh/Population expended by country.

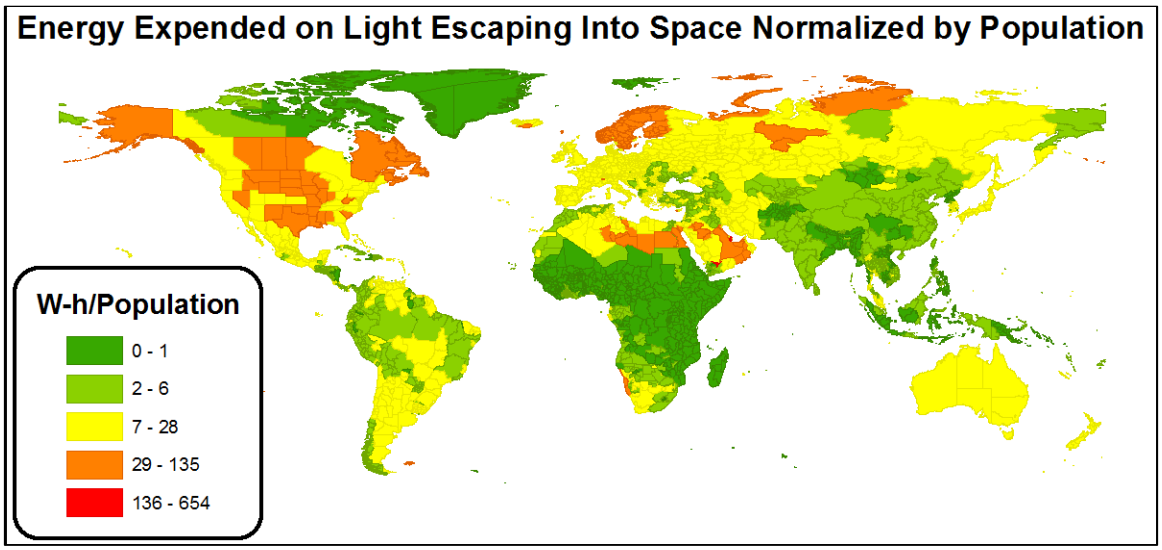

Figure 23. Map of states Wh/Population expended by state, states in the red category are difficult to discern and consist of: San Andres y Providencia, Colombia; Jarayan al Batnah, Qatar; Al Khawr, Qatar; Guantanamo Bay, United States; Ash Shamal, Qatar; Madinat Hamad, Bahrain; Al Jumayliyah, Qatar; Al Jawf, Yemen; Al Ghuwayriyah, Qatar.

The US EIA publishes a listing of international electricity prices and fuel costs online (US-Energy-Information-Administration, 2008). This data is broken down by electricity costs for industry and for households in US Dollars per kWh. Data is not available for all countries and in some countries only data for household or industry is available. The reported values for household cost and industry cost were averaged or if only one was reported that number was taken. The results was multiplied by the kWh estimated using the nighttime lights imagery. A map of the cost per hour of light shined skyward as estimated from the DMSP OLS is shown in Figure 24. The United States is the highest with a cost of approximately $1,000,000 spent to light the night sky during the time of observation by the sensor. Over the course of a year this adds up to $365 million. If we assume that this quantity of light is shone into the night sky for 8 hours a

night the costs rise to $2.92 billion per year. The numbers for all countries with available data on energy costs are reported in Table 7.

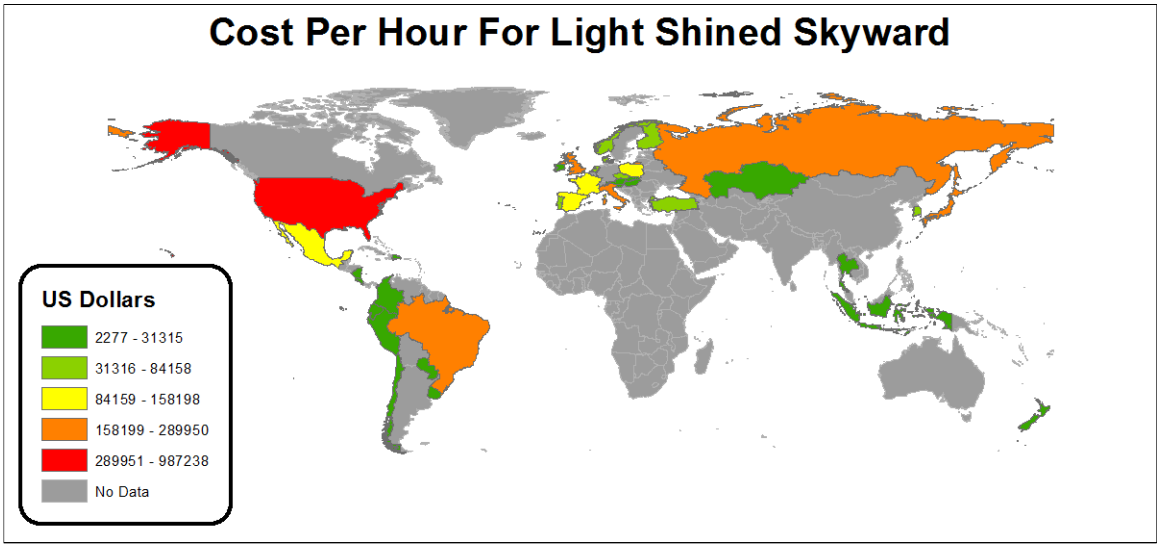

Figure 24: Map of the cost associated with producing the estimated Wh.

Table 7: Cost per hour for light shined skyward by country in US Dollars.

Country	Average Cost/kWh	kWh	Cost/Hour
Austria	0.1775	160172	$28,431
Brazil	0.1455	1387160	$201,832
Chile	0.17	134320	$22,834
Colombia	0.13	194124	$25,236
Costa Rica	0.095	34474	$3,275
Czech Republic	0.171	256457	$43,854
Denmark	0.396	134221	$53,152
Dominican Republic	0.1715	30053	$5,154
Ecuador	0.082	76985	$6,313
Finland	0.1345	625710	$84,158
France	0.1145	1260700	$144,350
Hungary	0.197	126089	$24,840
Indonesia	0.0625	262432	$16,402
Ireland	0.2265	138256	$31,315
Italy	0.2975	974621	$289,950
Japan	0.206	1295440	$266,861

Country	Average Cost/kWh	kWh	Cost/Hour
Kazakhstan	0.0455	240674	$10,951
South Korea	0.0745	501377	$37,353
Mexico	0.111	1017800	$112,976
Netherlands	0.243	239584	$58,219
New Zealand	0.1175	50496	$5,933
Nicaragua	0.179	12908	$2,311
Norway	0.114	462715	$52,750
Paraguay	0.06	37950	$2,277
Peru	0.1065	91189	$9,712
Poland	0.156	1014090	$158,198
Portugal	0.1755	214459	$37,638
Russia	0.05	3903150	$195,158
Singapore	0.1655	21853	$3,617
Slovakia	0.197	75439	$14,861
Slovenia	0.1715	39849	$6,834
Spain	0.124	970396	$120,329
Thailand	0.0845	347105	$29,330
Turkey	0.152	500516	$76,078
United Kingdom	0.1885	1048560	$197,654
United States	0.09135	10807200	$987,238
Uruguay	0.133	31342	$4,168
Luxembourg	0.215	12815	$2,755

These estimates are based on a number of assumptions. First, that all lights around the world have similar lumens to watts ratio as high pressure sodium lamps. Second, that all lighting types in use around the world have similar atmospheric transmission characteristics to the high pressure sodium lamps used in this study. High pressure and low pressure sodium lamps are estimated to account for 62% of outdoor lighting (Waide & Tanishima, 2006). It is known that many light sources commonly in use such as metal halide, mercury vapor, halogen, and incandescent have a lower lumens per watt ratio than high pressure sodium lamps. According to estimates the outdoor lights not provided by

high or low pressure sodium is 30% mercury vapor lamps, 6% metal halide lamps and the remaining 2% is made up mostly of a combination of halogen and incandescent lamps (Waide & Tanishima, 2006). This suggests that these estimates may be lower than the actual usage since all these lighting types are used in various parts of the world. High pressure sodium lamps also likely transmit more energy from the source to the OLS sensor as the peak intensity is in the red portion of the visible spectrum. This means low Rayleigh scattering compared to other light sources that have higher energy output in the green and blue portions of the visible spectrum. Also, the peak energy of the high pressure sodium lamps aligns with the peak sensitivity of the OLS sensor. This also suggests that the estimates here maybe low compared to the actual numbers.

A 2006 study by the International Energy Agency reports that outdoor stationary lighting used 218TWh of electricity in 2005 (Waide & Tanishima, 2006). While some of the light observed by the OLS may be escaping through windows from indoors, the clear majority of this light is from outdoor stationary lighting. The estimates reported here suggest that 140.37TWh of electricity is emitted into the sky based on the estimated Wh from the nighttime lights imagery and an assumption that that number is maintained for 8 hours per night each night of the year. This suggests that 150% of the energy used for outdoor lighting ends up lighting the sky. This number accounts for both light that is poorly directed and wasted into the sky at night as well as light directed at the ground and reflected back up into the sky. Although the reflected light is likely a small percentage of the total light emitted skyward at night it should be considered in analyzing these numbers.

Conclusions

In areas with no existing light it is possible to create a point source of light capable of being observed by the DMP OLS using a portable light consisting of high pressure sodium lamps. Additionally, the brightness of these point sources observed in the imagery correlate with the radiance values observed by the sensor. This capability allows for the estimation of the energy being expended each night by light sources around the globe that light up the night sky. These estimates show that the USA is by far the leading user of energy that lights the night sky followed by China and Russia at approximately 40% of the energy used by the USA and then India and Canada at approximately 20% of the energy used by the USA. By these estimates the USA expends roughly 10.8GWh on light that escapes into the sky at night, assuming this occurs for a period of eight hours each night this totals 86.4GWh per night.

More research is needed to further improve these estimates. There are two key areas for improvement over this study. First, given the varying efficiencies of different types of lamps used around the world to light cities it would be valuable to carry out this study with multiple lamp types. The varying lamp types in use have different atmospheric transmission properties and the sensitivity of the OLS to light in different portions of the visible spectrum also varies. Including mercury vapor, metal halide, halogen, and incandescent lamps in the field experiments would help improve the estimates. Second, it would be valuable to include measures of global atmospheric transmission to account for differences in the energy that is transmitted from the ground to the sensor in different parts of the world. These estimates may also be improved by applying the methodology

presented here using data from the Visible Infrared Imaging Radiometer Suite (VIIRS) (NASA, 2012) or the proposed Nightsat mission (Elvidge et al., 2007a; Elvidge et al., 2007c) rather than DMSP OLS imagery.

These estimates indicate very large amounts of energy are being used on light that is emitted into the sky rather than its intended purpose of lighting the ground in inhabited areas. In the US this wasted energy accounts for an estimated $2.92 billion per year. These results are alarming given the ecological impacts of light at night, the impacts of increased energy usage on our carbon footprint, the aesthetic loss of clearly viewing the night sky, and the possible economic savings from lower energy consumption. These estimates suggest that more effort should be expended on designing lights that concentrate the output downward to its intended audience with less energy escaping into the night sky.

Chapter Five: Summary

Review

The goal of this research was to address several questions.

1. Can a portable lighting source be used to further our understanding of the DMSP OLS, specifically the minimum detection brightness?

2. Can a portable light source be used as an active target for assessing the geolocation accuracy of the DMSP OLS?

3. Can a portable lighting source be used as an active calibration device on the ground for inter-annual and inter-satellite calibration of the DMSP OLS?

4. Can a portable lighting system be used to estimate the watts expended nightly on light that is shined in the sky.

In the following sections the answers to each of these questions will be reviewed.

Feasibility of a Portable Light to Calibrate the DMSP OLS

The first question set forth was "Can a portable lighting source be used to further our understanding of the DMSP OLS, specifically the minimum detection brightness?" Although early tests with halogen lamps and spotlights were unsuccessful, using commercially available high pressure sodium lamps this question was answered affirmatively. It has been determined that a portable lighting source consisting of high pressure sodium lamps can be used as an active calibration target for inter-annual and inter-satellite calibration of the DMSP OLS.

In answering this question objective one and two were also answered. Objective one sought to determine if a portable lighting system could be observed by the OLS. The

field experiments conducted achieved this objective. Furthermore objective two sought to determine the minimal detectable brightness of the OLS. Although more research is needed in this area valuable conclusions were made. First, using eight 1000W high pressure sodium lamps it is possible to saturate the OLS in the fine data. Additionally, it is possible to achieve DNs as high as 48 in the smooth data. Second, using only one 1000W high pressure sodium lamp it is possible to observe the portable light in both fine and smooth data.

When using only one 1000W high pressure sodium lamp the observed DNs fall into the single digits in both the fine and smooth data. Only two experiments were tried with less than 1000W of high pressure sodium light. In each of these trials three 250W high pressure sodium lamps were used. These tests were unsuccessful, but there are a number of factors that could have accounted for this including weather/atmospheric conditions, sensor gain, and scan angle. 1000W of high pressure sodium (approximately 140,000 lumens or approximately 93 100W incandescent light bulbs) may be the minimum detectable brightness. Furthermore, an assessment of the data was conducted that suggest the actual minimum detectable brightness may be approximately 900W of high pressure sodium for smooth data and approximately 600W of high pressure sodium for fine data. Due to the limited field experiments below 1000W, more trials should be conducted before a firm conclusion is drawn.

Assessing the Geolocation Accuracy of the DMSP OLS

Question two (objective three) aimed to determine if a portable light source be used as an active target for assessing the geolocation accuracy of the DMSP OLS. This was determined to be feasible and generated an easily repeatable process for such

assessments. By measuring the distance between the observed location of the light in DMSP OLS imagery and the recorded GPS location of the light the geolocation accuracy for satellites F16 and F18 was determined. Across both satellites the mean distance was 2.9km and the median was 2.81km. The mean bearing was -0.05° (measured between -180° and 180°) and the median was also -0.05°. This represents a shift of just over one smooth pixel to the north or five fine pixels. For both satellites the shift appears to be systematic in nature suggesting that the cause of the error is common to both satellites.

Individually satellites F16 and F18 had slightly different results, but the results were very close. For satellite F16 the mean distance measured between the recorded location of the light and the observed location was 2.49km with the bearing of -0.05°. The median distance was 2.72km and the median bearing was -0.03°. For satellite F18 the mean distance measured between the recorded location of the light and the observed location was 2.88km with a mean of -0.06°. The median distance was 2.75km and the median bearing was -0.07°. It would be valuable to conduct future studies in multiple regions of the world to determine if the systematic shift observed in North America is similar around the globe.

Anecdotal evidence from NGDC has found that annual composites of DMSP OLS imagery require a one smooth pixel shift to the south to be registered with other datasets of similar scale and global coverage. This anecdotal evidence is in agreement with the numbers found in this study. Going forth these results lend credence to a one smooth pixel shift to the south for DMSP OLS annual composites compiled using data from satellite F16 or F18.

Inter-calibration of the DMSP OLS

Question three (objective four) sought to create an inter-annual and inter-satellite calibration of the DMSP OLS using a portable light as an active ground target to calibrate the observations. Each night that a successful observation was made the amount of light used was recorded along with the DN, gain, scan angle, satellite, and spatial resolution of the data. Using these observations a linear regression model was constructed to predict radiance with using the amount of light used (measured in watts), the satellite, the spatial resolution, and the optical depth (1/distance to sensor^2).

When modeling both F16 and F18 together this model produced an R^2 of 0.61. When the model was applied for satellite F16 the R^2 was 0.72 and for F18 the R^2 was 0.72. A higher R^2 value was achieved when models were built independently for each satellite suggesting a significant difference in the current spectral response of the OLS on the two satellites. Using these models it should be possible to adjust the values in imagery collected from each satellite in order to make more realistic comparisons between the data collected. Additionally, over time this process should support the determination of adjustments of the data to improve the quality of temporal data comparisons.

These models might be improved if a detailed atmospheric model for each night was included in the model. Additionally, to make this methodology more useful it would be valuable to have a permanent installation that could be easily used at regular intervals. This would allow for a more accurate reporting of changes over time and between satellites.

Assessing the Energy Consumed to Light the Night Sky

The fourth and final question asked "can a portable lighting system be used to estimate the watts expended nightly on light that is shined in the sky?" Using the methods established in this research this question and objective five are easily answered. Using the linear regression models from the inter-calibration portion of the study the radiance of DMSP OLS data can be converted to watts. The total energy consumption for lighting the night sky globally was measured along with statistics by country and state as well as annual cost for countries where electricity rates were available.

The USA is by far the leading user of energy that lights the night sky by these estimates. It is followed by China and Russia using approximately 40% of the energy used by the USA. India and Canada rank fourth and fifth and use approximately 20% of the energy used by the USA. According to these estimates the USA expends roughly 10.8GWh on lighting the night sky, and based on an assumption that this occurs for a period of eight hours each night this totals 86.4GWh per night. This equates to an annual cost of $2.9 billion in the USA for the year 2008.

These estimates may be imperfect due to the assumption the all light emitted into the sky at night is created by high pressure sodium lamps. While it is reported that high pressure and low pressure sodium lamps are estimated to account for 62% of outdoor lighting (Waide & Tanishima, 2006) the remainder is made up of mercury vapor, metal halide, halogen, incandescent, and other types of lamps. These lamps have lower lumens per watt ratios then high pressure sodium and different atmospheric transmission qualities. These estimates could be improved by including other lighting types in the

assessments. Additionally, the inclusion of data on atmospheric transmission would be valuable in improving these estimates.

Conclusion

This research has produced an easily repeatable methodology for creating an active point source capable of being detected by the DMSP OLS. This target can be created with commercially available high pressure sodium lamps and can be easily transported in a utility trailer along with gas generators capable of powering the array for upwards of five hours. This portable light source has a wide array of application to DMSP OLS imagery.

Using a portable light source such as the one defined here:

1. The minimum detectable brightness of the OLS can be documented.
2. Geolocation accuracy of the DMSP OLS can be determined.
3. Inter-annual and inter-satellite calibrations can be performed to enhance the quality of comparisons made using imagery from different time periods or different satellites.
4. The total energy expended to light the night sky, rather than the ground for which it is intended, can be estimated.

This methodology also has applicability beyond the DMSP OLS. The VIIRS, which is also capable of observing nocturnal light emissions, could also benefit from this research. The geolocation assessment and inter-calibration methods should be applicable and the increased spatial and spectral resolution of VIIRS should allow for enhanced estimates of the energy used to light the night sky. The same is true of the proposed Nightsat program, which could benefit from the geolocation and inter-satellite calibration process defined here. In addition, Nightsat could provide even more precise estimates of

the energy expended skyward at night. Nightsat will have multiple bands allowing one to begin discerning where different types of light are being used. This information used in conjunction with portable lights using multiple lamp types would increase the accuracy of the estimates by allowing the appropriate conversion from radiance to watts to be used for different regions of the globe.

More research is needed to improve upon the capabilities defined here. However, a valuable resource has been reported and can be easily used by others to conduct similar studies. The research presented here has presented a first estimate of the minimum detectable brightness by the DMSP OLS, updated geolocation accuracy reports, a new method for inter-calibration, and has also presented a first look at the total energy consumed lighting the night sky.

References

Acharya, L., & Fenton, M. B. (1999). Bat attacks and moth defensive behaviour around street lights. *Canadian Journal of Zoology-Revue Canadienne De Zoologie, 77*(1), 27-33.

Anderson, S. J., Tuttle, B. T., Powell, R. L., & Sutton, P. C. (2010). Characterizing relationships between population density and nighttime imagery for Denver, Colorado: issues of scale and representation. *International Journal of Remote Sensing, 31*(21), 5733-5746.

Baker, B. J., & Richardson, J. M. L. (2006). The effect of artificial light on male breeding-season behaviour in green frogs, Rana clamitans melanota. *Canadian Journal of Zoology-Revue Canadienne De Zoologie, 84*(10), 1528-1532.

Balk, D., Brickman, M., Anderson, B., Pozzi, F., & Yetman, G. (2005). Mapping global urban and rural population distributions [Electronic Version]. *FAO Environment and Natural Resources Working Paper*, 24. Retrieved 4-28-2012 from http://sedac.ciesin.columbia.edu/gpw/docs/GISn.24_web_gpwAnnex.pdf.

Balk, D., & Yetman, G. (2004). The Global Distribution of Population: Evaluating the gains in resolution refinement. Retrieved 4-29-2012, 2012, from http://sedac.ciesin.columbia.edu/gpw/docs/gpw3_documentation_final.pdf

Balk, D., Yetman, G., & de Sherbinin, A. (2010). *Construction of Gridded Population and Poverty Data Sets from Different Data Sources.* Paper presented at the Proceedings of European Forum for Geostatistics Conference, Tallinn, Estonia.

Bartholome, E., & Belward, A. S. (2005). GLC2000: a new approach to global land cover mapping from Earth observation data. *International Journal of Remote Sensing, 26*(9), 1959-1977.

Baugh, K., Elvidge, C., Ghosh, T., & Ziskin, D. (2010). *Development of a 2009 Stable Lights Product using DMSP-OLS data.* Paper presented at the Proceedings of the 30th Asia-Pacific Advanced Network Meeting, Hanoi, Vietnam.

Bertolotti, L., & Salmon, M. (2005). Do embedded roadway lights protect sea turtles? *Environmental Management 36*(5), 702-710.

Bhaduri, B., Bright, E., Coleman, P., & Dobson, J. (2002). LandScan: Locating People is What Matters. *Geoinformatics, 5*(2), 34-37.

Blake, D., Hutson, A. M., Racey, P. A., Rydell, J., & Speakman, J. R. (1994). Use of Lamplit Roads by Foraging Bats in Southern England. *Journal of Zoology, 234*(3), 453-462.

Boldogh, S., Dobrosi, D., & Samu, P. (2007). The effects of the illumination of buildings on house-dwelling bats and its conservation consequences. *Acta Chiropterologica, 9*(2), 527-534.

Chand, T. R. K., Badarinath, K. V., Prasad, V. K., Murthy, M. S. R., Elvidge, C. D., & Tuttle, B. T. (2006). Monitoring forest fires over the Indian region using Defense Meteorological Satellite Program-Operational Linescan System nighttime satellite data. *Remote Sensing of Environment, 103*(2), 165-178.

Chand, T. R. K., Badarinath, K. V. S., Murthy, M. S. R., Rajshekhar, G., Elvidge, C. D., & Tuttle, B. T. (2007). Active forest fire monitoring in uttaranchal state, India

using multi-temporal DMSP-OLS and MODIS data. *International Journal of Remote Sensing, 28*(10), 2123-2132.

CIESIN, IFPRI, The-World-Bank;, & CIAT. (2004). Global Rural-Urban Mapping Project (GRUMP), Alpha Version: Urban Extents. Retrieved 4-29-2012, 2012, from http://sedac.ciesin.columbia.edu/gpw

Cova, T. J., Sutton, P. C., & Theobald, D. M. (2004). Exurban change detection in fire-prone areas with nighttime satellite imagery. *Photogrammetric Engineering and Remote Sensing, 70*(11), 1249-1257.

Cuartero, A., Felicisimo, A. M., Polo, M. E., Caro, A., & Rodriguez, P. G. (2010). Positional Accuracy Analysis of Satellite Imagery by Circular Statistics. *Photogrammetric Engineering and Remote Sensing, 76*(11), 1275-1286.

Doll, C. N. H., Muller, J. P., & Elvidge, C. D. (2000). Night-time imagery as a tool for global mapping of socioeconomic parameters and greenhouse gas emissions. *Ambio, 29*(3), 157-162.

Dolloff, J., & Settergren, R. (2010). An Assessment of WorldView-1 Positional Accuracy based on Fifty Contiguous Stereo Pairs of Imagery. *Photogrammetric Engineering and Remote Sensing, 76*(8), 935-943.

Elvidge, C. D., Baugh, K., Tuttle, B., Ziskin, D., & Ghosh, T. (2009a). *Satellite Observation of Heavily Lit Fishing Boat Activity in the Coral Triangle Region.* Paper presented at the Proceedings of the 30th Asian Conference on Remote Sensing, Beijing, China.

Elvidge, C. D., Baugh, K. E., Dietz, J. B., Bland, T., Sutton, P. C., & Kroehl, H. W. (1999). Radiance calibration of DMSP-OLS low-light imaging data of human settlements. *Remote Sensing of Environment, 68*(1), 77-88.

Elvidge, C. D., Baugh, K. E., Hobson, V. R., Kihn, E. A., & Kroehl, H. W. (1998). Detection of Fires and Power Outages Using DMSP-OLS Data. In R. S. Lunetta & C. D. Elvidge (Eds.), *Remote Sensing Change Detection: Environmental Monitoring Methods and Applications* (pp. 123-135). Chelsea, Michigan, USA: Ann Arbor Press.

Elvidge, C. D., Baugh, K. E., Hobson, V. R., Kihn, E. A., Kroehl, H. W., Davis, E. R., et al. (1997a). Satellite inventory of human settlements using nocturnal radiation emissions: A contribution for the global toolchest. *Global Change Biology, 3*(5), 387-395.

Elvidge, C. D., Baugh, K. E., Kihn, E. A., Kroehl, H. W., & Davis, E. R. (1997b). Mapping city lights with nighttime data from the DMSP operational linescan system. *Photogrammetric Engineering and Remote Sensing, 63*(6), 727-734.

Elvidge, C. D., Baugh, K. E., Kihn, E. A., Kroehl, H. W., Davis, E. R., & Davis, C. (1997c). Relation between satellite observed visible - near infrared emissions, population, and energy consumption. *International Journal of Remote Sensing, 18*, 1373-1379.

Elvidge, C. D., Cinzano, P., Pettit, D. R., Arvesen, J., Sutton, P., Small, C., et al. (2007a). The Nightsat mission concept. *International Journal of Remote Sensing, 28*(12), 2645-2670.

Elvidge, C. D., Erwin, E. H., Baugh, K. E., Tuttle, B. T., Howard, A. T., Pack, D. W., et al. (2007b). Satellite data estimate worldwide flared gas volumes. *Oil & Gas Journal, 105*(42), 50-+.

Elvidge, C. D., Hobson, V. R., Baugh, K. E., Dietz, J. B., Shimabukuro, Y. E., Krug, T., et al. (2001a). DMSP-OLS estimation of tropical forest area impacted by surface fires in Roraima, Brazil: 1995 versus 1998. *International Journal of Remote Sensing, 22*(14), 2661-2673.

Elvidge, C. D., Imhoff, M. L., Baugh, K. E., Hobson, V. R., Nelson, I., Safran, J., et al. (2001b). Night-time lights of the world: 1994-1995. *Isprs Journal of Photogrammetry and Remote Sensing, 56*(2), 81-99.

Elvidge, C. D., Keith, D. M., Tuttle, B. T., & Baugh, K. E. (2010). Spectral Identification of Lighting Type and Character. *Sensors, 10*(4), 3961-3988.

Elvidge, C. D., Milesi, C., Dietz, J. B., Tuttle, B. T., Sutton, P. C., Nemani, R., et al. (2004a). U.S. constructed area approaches the size of Ohio. *EOS Transactions, American Geophysical Union, 85*, 233.

Elvidge, C. D., Nelson, I., Hobson, V. R., Safran, J., & Baugh, K. E. (2001c). Detection of fires at night using DMSP-OLS data. In F. J. G. Ahern, J.G.; Justice, C.O. (Ed.), *Global and Regional Vegetation Fire Monitoring from Space: Planning a Coordinated International Effort* (pp. 125-144). The Hague, The Netherlands: SPB Academic Publishing bv.

Elvidge, C. D., Safran, J., Nelson, I. L., Tuttle, B. T., Hobson, V. R., Baugh, K. E., et al. (2004b). Area and position accuracy of DMSP nighttime lights data. In L. R.S. & J. G. Lyon (Eds.), *Remote Sensing and GIS Accuracy Assessment* (pp. 281-292): CRC Press.

Elvidge, C. D., Safran, J., Tuttle, B., Sutton, P., Cinzano, P., Pettit, D., et al. (2007c). Potential for global mapping of development via a nightsat mission. *GeoJournal, 69*(1-2), 45-53.

Elvidge, C. D., Sutton, P. C., Ghosh, T., Tuttle, B. T., Baugh, K. E., Bhaduri, B., et al. (2009b). A global poverty map derived from satellite data. *Computers & Geosciences, 35*(8), 1652-1660.

Elvidge, C. D., Sutton, P. C., Wagner, T. W., Ryzner, W., Vegelman, J. E., Goetz, S. J., et al. (2004c). Urbanization. In G. Gutman & e. al (Eds.), *Land Change Science* (pp. 315-328). Netherlands: Kluwer Academic Publishers.

Elvidge, C. D., Tuttle, B. T., Sutton, P. S., Baugh, K. E., Howard, A. T., Milesi, C., et al. (2007d). Global distribution and density of constructed impervious surfaces. *Sensors, 7*(9), 1962-1979.

Elvidge, C. D., Ziskin, D., Baugh, K. E., Tuttle, B. T., Ghosh, T., Pack, D. W., et al. (2009c). A Fifteen Year Record of Global Natural Gas Flaring Derived from Satellite Data. *Energies, 2*(3), 595-622.

Fragkias, M., & Seto, K. C. (2007). Urban Land-Use Change, Models, Uncertainty, and Policymaking in Rapidly Growing Developing World Cities: Evidence From China. In R. J. Aspinall & M. J. Hill (Eds.), *Land Use Change Science: Science, Policy, and Management* (pp. 139-162). Boca Raton: CRC Press.

Ghosh, T., Anderson, S., Powell, R. L., Sutton, P. C., & Elvidge, C. D. (2009). Estimation of Mexico's Informal Economy and Remittances Using Nighttime Imagery. *Remote Sensing of Environment, 1*(3), 418-444.

Ghosh, T., Elvidge, C. D., Sutton, P. C., Baugh, K. E., Ziskin, D., & Tuttle, B. T. (2010a). Creating a Global Grid of Distributed Fossil Fuel CO(2) Emissions from Nighttime Satellite Imagery. *Energies, 3*(12), 1895-1913.

Ghosh, T., Powell, R., Elvidge, C. D., Baugh, K. E., Sutton, P. C., & Anderson, S. (2010b). Shedding light on the global distribution of economic activity. *The Open Geography Journal, 3*(15), 148-161.

Ghosh, T., Powell, R. L., Anderson, S., Sutton, P. C., & Elvidge, C. D. (2010c). Informal Economy And Remittance Estimates of India Using Nighttime Imagery. *International Journal of Ecological Economics & Statisitics, 17*.

Goldewijk, K. K. (2001). Estimating global land use change over the past 300 years: The HYDE Database. *Global Biogeochemical Cycles, 15*(2), 417-433.

Goldewijk, K. K., & Ramankutty, N. (2004). Land cover change over the last three centuries due to human activities: The availability of new global data sets. *Geojournal, 61*, 335-344.

Henderson, M., Yeh, E. T., Gong, P., Elvidge, C., & Baugh, K. (2003). Validation of urban boundaries derived from global night-time satellite imagery. *International Journal of Remote Sensing, 24*(3), 595-609.

Imhoff, M. L., Lawrence, W. T., Elvidge, C. D., Paul, T., Levine, E., & Privalsky, M. V. (1997a). Using nighttime DMSP/OLS images of city lights to estimate the impact of urban land use on soil resources in the United States. *Remote Sensing of Environment, 59*(1), 105-117.

Imhoff, M. L., Lawrence, W. T., Stutzer, D. C., & Elvidge, C. D. (1997b). A technique for using composite DMSP/OLS "city lights" satellite data to map urban area. *Remote Sensing of Environment, 61*(3), 361-370.

International-Dark-Sky-Association. (2012). Directory of State and Country Lighting Laws. Retrieved 4-28-2012, 2012, from http://www.darksky.org/index.php?option=com_content&view=article&id=678

Karnad, D., Isvaranb, K., Karc, C. S., & Shanker, K. (2009). Lighting the way: Towards reducing misorientation of olive ridley hatchlings due to artificial lighting at Rushikulya, India. *Biological Conservation, 142*(10), 2083-2088.

Kloog, I., Haim, A., Stevens, R. G., Barchana, M., & Portnov, B. A. (2008). Light at Night Co-distributes with Incident Breast but not Lung Cancer in the Female Population of Israel. *Chronobiology International, 25*(1), 65-81.

Lee, J. (2008). Bright Lights at Night, Perhaps Not Such a Delight. *City Room* Retrieved April 22, 2012, from http://cityroom.blogs.nytimes.com/2008/02/25/bright-lights-at-night-perhaps-not-such-a-delight/#

Lo, C. P. (2001). Modeling the population of China using DMSP operational linescan system nighttime data. *Photogrammetric Engineering and Remote Sensing, 67*(9), 1037-1047.

Lo, C. P. (2002). Urban indicators of China from radiance-calibrated digital DMSP-OLS nighttime images. *Annals of the Association of American Geographers, 92*(2), 225-240.

Longcore, T., & Rich, C. (2004). Ecological light pollution. *Frontiers in Ecology and the Environment, 2*(4), 191-198.

Lulla, K. (2003). Nighttime urban imagery from international space station: Potential applications for urban analyses and modeling. *Photogrammetric Engineering and Remote Sensing, 69*(9), 941-942.

Lyon, L. J., & Stickney, P. F. (1976). *Early vegetal succession following large northern Rocky Mountain wildfires.* Paper presented at the Tall Timbers Fire Ecology Conference.

Maxwell, M. R., Henry, A., Elvidge, C. D., Safran, J., Hobson, V. R., Nelson, I., et al. (2004). Fishery dynamics of the California market squid (Loligo opalescens), as measured by satellite remote sensing. *Fishery Bulletin, 102*(4), 661-670.

McNamara, D., Stephens, G., Ramsay, B., Prins, E., Csiszar, I., Elvidge, C., et al. (2002). Fire detection and monitoring products at the National Oceanic and Atmospheric Administration. *Photogrammetric Engineering and Remote Sensing, 68*(8), 774-775.

Milesi, C., Elvidge, C. D., Nemani, R. R., & Running, S. W. (2003). Assessing the impact of urban land development on net primary productivity in the southeastern United States. *Remote Sensing of Environment, 86*, 273 – 432.

Milesi, C., Running, S. W., Elvidge, C. D., Dietz, J. B., Tuttle, B. T., & Nemani, R. R. (2005). Mapping and modeling the biogeochemical cycling of turf grasses in the United States. *Environmental Management, 36*(3), 426-438.

Nagatani, I. (2010, August 9 - 13). *A methodology to create DMSP-OLS night-time mosaic image for monitoring fishing boats.* Paper presented at the Proceedings of the 30th Asia-Pacific Advanced Network Meeting, Hanoi, Vietnam.

NASA. (2012). NASA's NPP Satellite Acquires First VIIRS Image. Retrieved March 30, 2012, 2012, from http://www.nasa.gov/mission_pages/NPP/news/viirs-firstlight.html

Navara, K. J., & Nelson, R. J. (2007). The dark side of light at night: physiological, epidemiological, and ecological consequences. *Journal of Pineal Research, 43*(3), 215-224.

NOAA/NGDC. (2012). Earth Observation Group - Defense Meteorological Satellite Program. Retrieved March 30, 2012, 2012, from http://www.ngdc.noaa.gov/dmsp/

O'Hara, C. G., Cary, T., & Schuckman, K. (2010). Integrated Technologies for Orthophoto Accuracy Verification and Review. *Photogrammetric Engineering and Remote Sensing, 76*(10), 1097-1103.

Pauley, S. M. (2004). Lighting for the human circadian clock: recent research indicates that lighting has become a public health issue. *Medical Hypotheses, 63*(4), 588-596.

Philibosian, R. (1976). Disorientation of Hawksbill Turtle Hatchlings, Eretmochelys-Imbricata, by Stadium Lights. *Copeia, 4*, 824.

Potere, D., & Schneider, A. (2007). A critical Look at representations of urban areas in global maps. *GeoJournal, 69*(1-2), 55-80.
Powell, R. L., Roberts, D. A., Dennison, P. E., & Hess, L. L. (2007). Sub-pixel mapping of urban land cover using multiple endmember spectral mixture analysis: Manaus, Brazil. *Remote Sensing of Environment, 106*(2), 253-267.
Prasad, V. K., Kant, Y., Gupta, P. K., Elvidge, C., & Badarinath, K. V. S. (2002). Biomass burning and related trace gas emissions from tropical dry deciduous forests of India: A study using DMSP-OLS data and ground-based measurements. *International Journal of Remote Sensing, 23*(14), 2837-2851.
Qiao, G., Wang, W., Wu, B., Liu, C., & Li, R. (2010). Assessment of Geo-positioning Capability of High Resolution Satellite Imagery for Densely Populated High Buildings in Metropolitan Areas. *Photogrammetric Engineering and Remote Sensing, 76*(8), 923-934.
Salmon, M., & Witherington, B. E. (1995). Artificial lighting and seafinding by loggerhead hatchlings: Evidence for lunar modulation. *Copeia, 4*, 931-938.
Schneider, A., Friedl, M. A., McIver, D. K., & Woodcock, C. E. (2003). Mapping urban areas by fusing multiple sources of coarse resolution remotely sensed data. *Photogrammetric Engineering and Remote Sensing, 69*(12), 1377-1386.
Small, C., Pozzi, F., & Elvidge, C. D. (2005). Spatial analysis of global urban extent from DMSP-OLS night lights. *Remote Sensing of Environment, 96*(3-4), 277-291.
Surazakov, A., & Aizen, V. (2010). Positional Accuracy Evaluation of Declassified Hexagon KH-9 Mapping Camera Imagery. *Photogrammetric Engineering and Remote Sensing, 76*(5), 603-608.
Sutton, P. (1997). Modeling population density with night-time satellite imagery and GIS. *Computers Environment and Urban Systems, 21*(3/4), 227–244.
Sutton, P., Roberts, C., Elvidge, C., & Meij, H. (1997). A comparison of nighttime satellite imagery and population density for the continental united states. *Photogrammetric Engineering and Remote Sensing, 63*(11), 1303-1313.
Sutton, P. C., Cova, T., & Elvidge, C. (2006). Mapping Exurbia in the conterminous United States using Nighttime Satellite Imagery. *Geocarto International, 20*(2).
Sutton, P. C., Elvidge, C., & Obremski, T. (2003). Building and evaluating models to estimate ambient population density. *Photogrammetric Engineering and Remote Sensing, 69*(5), 545-553.
Turner, M. G., Romme, W. H., Gardner, R. H., & Hargrove, W. W. (1997). Effects of Fire Size And Pattern on Early Succession in Yellowstone National Park. *Ecological Monographs, 67*(4), 411-433.
United-Nations-Population-Fund. (2008). *State of World Population 2008*

US-Energy-Information-Administration. (2008, 4-28-2012). International Electricity Prices and Fuel Costs. from http://www.eia.gov/emeu/international/electricityprice.html
Waide, P., & Tanishima, S. (2006). *Light's Labour's Lost: Policies for Energy-efficient Lighting*. Paris: Organisation For Economic Co-Operation And Development/International Energy Agency.

Weeks, J. R. (1999). *Population: An Introduction to Concepts and Issues*. Belmont: Wadsworth Publishing Company.

Wiltschko, W., Munro, U., Ford, H., & Wiltschko, R. (1993). Red-Light Disrupts Magnetic Orientation of Migratory Birds. *Nature, 364*(6437), 525-527.

Wiltschko, W., & Wiltschko, R. (1999). The effect of yellow and blue light on magnetic compass orientation in European robins, Erithacus rubecula. *Journal of Comparative Physiology a-Sensory Neural and Behavioral Physiology, 184*(3), 295-299.

Witmer, F. D. W., & O'Loughlin, J. (2011). Detecting the Effects of Wars in the Caucasus Regions of Russia and Georgia Using Radiometrically Normalized DMSP-OLS Nighttime Lights Imagery. *Giscience & Remote Sensing, 48*(4), 478-500.

Yang, L. M., Huang, C. Q., Homer, C. G., Wylie, B. K., & Coan, M. J. (2003). An approach for mapping large-area impervious surfaces: synergistic use of Landsat-7 ETM+ and high spatial resolution imagery. *Canadian Journal of Remote Sensing, 29*(2), 230-240.

Ziskin, D., Baugh, K., Hsu, F., Ghosh, T., & Elvidge, C. (2010). *Methods Used For the 2006 Radiance Lights.* Paper presented at the Proceedings of the 30th Asia-Pacific Advanced Network Meeting, Hanoi, Vietnam.